Both the cultured cells and the mutant fish exhibited decreased cathepsin D enzymatic activity, fingerprint-like inclusion body formation, and neuronal death. These findings indicated that abnormalities in lysosome function are the primary defect in KRS/PARK9.

2. Results

2.1. Wild-type ATP13A2 localizes to the lysosome, but some disease-relevant variants localize to the endoplasmic reticulum

To investigate the subcellular localization of ATP13A2, we used an anti-V5 antibody and antibodies that recognize several markers of intracellular organelles to double label SH-SY5Y cells that stably expressed wild-type ATP13A2 fused to the V5 epitope (WT-V5). The WT-V5 signal largely colocalized with the signal of cathepsin D, a lysosomal aspartic protease (Fig. 1A and S1). Additionally, WT-V5 partially overlapped with makers of the Golgi apparatus (GM130), the late endosome (Rab7) and the autophagosome (LC3B), but not with the markers of the endoplasmic reticulum (ER) (GRP78), the mitochondria (Tom20), the early endosome (EEA1 and Rab5), or the exocytotic vesicles (Rab3 and 4) (Fig. 1A, B and S1). GFP signals in SH-SY5Y cells that stably expressed GFP-tagged wild-type ATP13A2 (GFP-WT) strongly colocalized with either of two lysosomal membrane proteins, Lamp2 (Fig. 1A and S1) or Lamp1 (data not shown). Furthermore, immunoelectron microscopy using ultrathin cryosections of GFP-WT SH-SY5Y cells confirmed that gold particles labeling GFP-WT (arrow head: 10 nm gold) and those labeling Lamp1 (arrow: 5 nm gold) co-localized on the lysosomal membrane (Fig. 1C). These data indicated that ATP13A2 is a resident protein of the lysosomal membrane.

Thus far, eight disease-associated mutations have been identified in the *ATP13A2* gene, including one that we described initially [3–8]. To determine whether the mutant proteins were mislocalized and whether any such mislocalization has etiological importance, we assessed the subcellular localization of five pathogenic protein variants (Fig. 2A). These mutants were each tagged with a V5 epitope and then transiently transfected into SH-SY5Y cells. To, first, characterize the subcellular distribution of KRS mutants, we separated cell homogenates by Percoll density gradient centrifugation. This Percoll gradient system separates dense lysosomes (near bottom) from lighter particles such as ER. We found that WT-V5 was mainly co-fractionated with lysosomal component (Lamp1 and cathepsin D; Fraction No. 13–16, Fig. 2B). However, an ATP13A2 variant that lacks exon 13 (1306 + 5G→A) but maintains the reading frame was co-fractionated not with lysosomal proteins but with GRP78 (Fraction No. 2–8, Fig. 2B): this finding indicated that the protein variant accumulated in the ER. Some other ATP13A2 pathogenic variants (F182L and G504R) also accumulated in the ER in a manner similar to the 1306 + 5G→A variant. In contrast, the other two pathogenic variants (T12M and G533R) were co-fractionated with lysosomal components, as was the WT protein. To, further, confirm the subcellular localization, we carried out double fluorescence immunocytochemistry of permeabilized SH-SY5Y cells by staining KRS mutants (V5), the ER marker (GRP78), the lysosomal marker (cathepsin D) and the mitochondria marker (Tom20). Along with immunoblotting of Percoll density gradient fractionation, immunofluorescence studies showed 1306 + 5G→A mutant, F182L and G504R colocalized with GRP78 and the other two variants (T12M and G533R) colocalized with cathepsin D as already reported [10–14] (Fig. 2C and S1). The expression levels of ATP13A2 mutant proteins that accumulated in the ER (F182L, G504R, and 1306 + 5G→A) were lower than that of the WT protein and MG132 inhibited degradation of the all ATP13A2 variants as well as that of the WT protein (Fig. 2D).

2.2. Stable knockdown of ATP13A2 induces cathepsin D deficiency and structures that resemble neuronal ceroid-lipofuscinosis deposits

To assess whether the loss of normal ATP13A2 functions has a causal role in PD pathogenesis, the expression of endogenous ATP13A2 was suppressed in SH-SY5Y cells by gene knockdown. By using antibodies that we generated (Fig. 3A), we showed that endogenous ATP13A2 protein levels in SH-SY5Y cells that stably expressed ATP13A2 shRNA (ATP13A2shRNA-1 or -2) were efficiently suppressed (Fig. 3B). Water soluble Tetrazolium salts (WST)-8 assay demonstrated that ATP13A2 knockdown caused a significant reduction of the cell growth in SH-SY5Y cells (Fig. 3B). Next, we determined the distribution and the morphology of lysosomes in SH-SY5Y cells subjected to ATP13A2 knockdown. Immunostaining of cathepsin D and Lamp2 indicated that ATP13A2 deficiency led to the assembly of lysosomes in the perinuclear region and decreased cathepsin D staining (Fig. S2). The protein amount of full length (52-kDa), immature (44-kDa) and mature (32-kDa) forms of cathepsin D of the cells expressing ATP13A2 shRNAs were all decreased together with the enzyme activity (Fig. 3C). To show the reduction of cathepsin D activity was indeed induced by the reduction of ATP13A2, not by the non-specific effect of shRNA, we generated shRNA-resistant species of ATP13A2. SH-SY5Y cells stably expressing ATP13A2 shRNAs that were transfected with shRNA resistant ATP13A2 showed comparable cathepsin D activity to the controls (Fig. S3A). The activity and amount of mature forms (25-kDa) of cathepsin B and L were also decreased in the knockdown cells line by ATP13A2 shRNA-1, but not shRNA-2, suggesting that the loss of ATP13A2 principally gives rise to the reduction of cathepsin D (Fig. 3C). Finally, analysis via transmission electron microscopy revealed that lysosome-like bodies became more numerous in ATP13A2 shRNAs expressing cells and that very immense high density structure appeared adjacent to the nucleus in these cells (Fig. 3D: a–h). High-magnification images revealed that the abnormal structures in these cells included fingerprint profiles-like structure (Fig. 3D: e), and these structures were very similar to the structure of the neurons in mice lacking cathepsin D [15]. The levels of LC3-II, autophagosome marker, in shRNA-1 transfected cells were increased (Fig. 3E) and p62 a substrate of autophagic degradation, was accumulated in both of the shRNA expressing lines (Fig. S3B), suggesting that an appearance of abnormal structure induced by ATP13A2 deficiency might be involved with impaired lysosomal proteolysis. Taken together, these findings indicated that loss of ATP13A2 led to lysosomal pathology and, more specifically, a reduction in cathepsin D activity.

2.3. Generation of an Atp13a2 mutant medaka fish

Next, we generated and evaluated medaka fish with an Atp13a2 mutation to investigate the mechanism of KRS/PARK9-associated neurodgeneration in vivo. The draft of the medaka genome contains only one identifiable ortholog of the human *ATP13A2* gene. We cloned the medaka *atp13a2* gene by RT-PCR and RACE, and it encoded a protein consisting of 1159 amino acids. The amino-acid sequence showed 51.3% homology to human ATP13A2 protein (Fig. S4A). To characterize medaka *atp13a2* expression, we used in situ hybridization to visualize medaka *atp13a2* mRNA. No signal was observed with the sense RNA probe. However, the anti-sense RNA probe resulted in diffuse signals in the gray matter of medaka brain (Fig. 4A). The telencephalon and diencephalon that contain the putative striatum and many dopaminergic neurons, respectively, were intensely labeled by the anti-sense probe. The optic tectum was also intensely labeled, but the hindbrain and spinal cord were scarcely labeled (Fig. 4A).

We then used TILLING (Targeting Induced Local Lesions In Genomes) method to generate an Atp13a2 mutant fish [16]. We

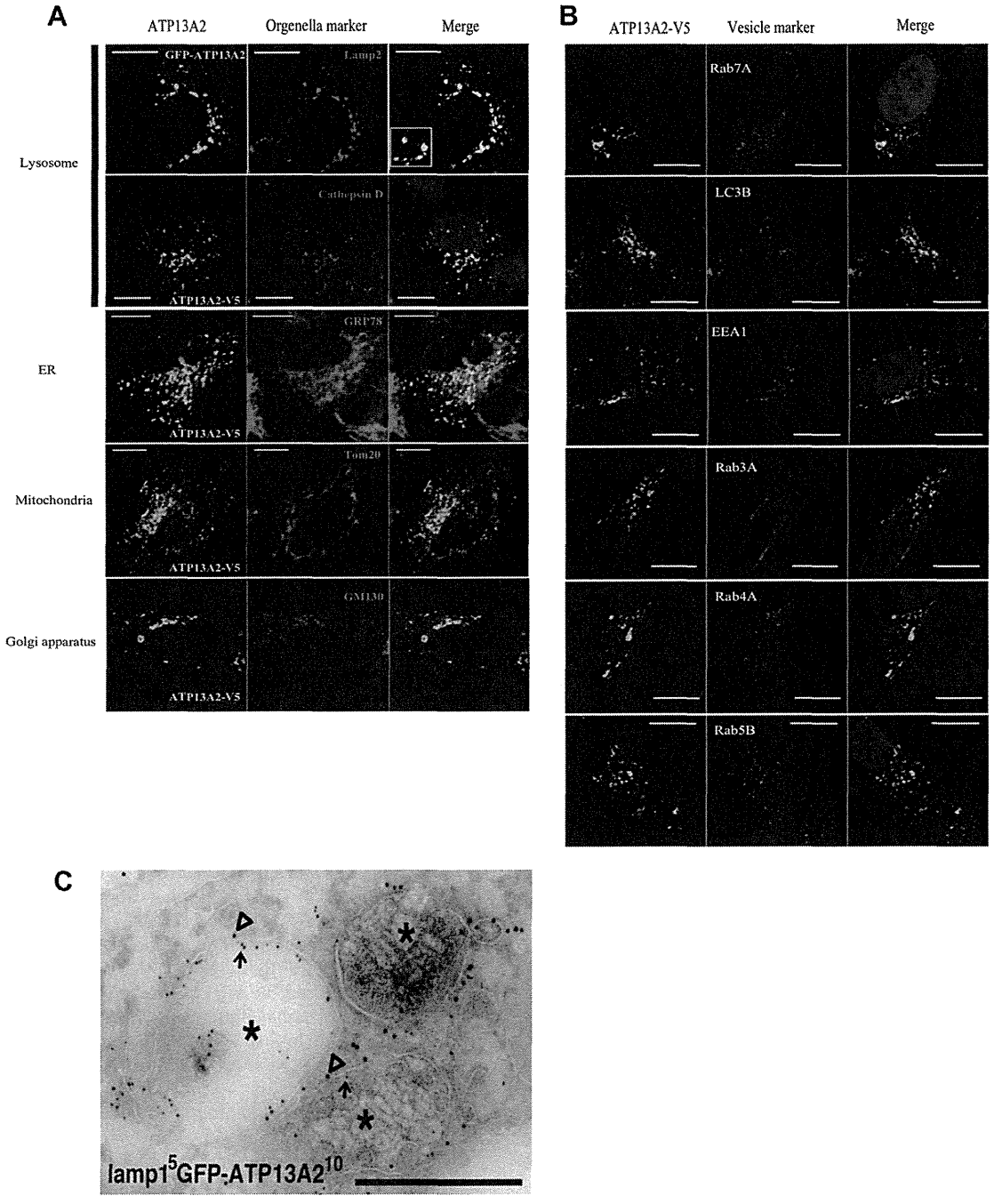

Fig. 1. Wild-type ATP13A2 localizes at lysosomal membranes. (A and B) WT-V5 and GFP-WT fusion proteins consistently co-localizes with Lamp2 and cathepsin D. Additionally, WT-V5 partially overlapped with GM130, Rab7 and LC3B. (Scale bar; 10 μm). (C) Immunoelectron microscopy using ultrathin cryosections. Double immunostaining of GFP-ATP13A2 (gold particles, 10 nm in diameter (open arrowheads)) and Lamp1 (gold particles, 5 nm in diameter (arrows)). Both types of immuno-gold label clearly localizes along the membranes around lysosomes (asterisks). (Scale bar; 0.5 μm).

sequenced the genomes of 5771 samples obtained from our ENU-mutagenized medaka library, and identified one mutation "IVS13, T-C, +2" that resulted in an aberrant splice donor site (Fig. 4B). The IVS13, T-C, +2 mutant from this strain was subjected to six sequential backcrosses to generate the mutant used in the following experiments. A cross between heterozygous "IVS13, T-C, +2" mutant pair resulted in wild-type fish (WT/WT), heterozygous mutants (WT/mt), and homozygous mutants (mt/mt) in Mendelian ratios. RT-PCR analysis revealed an abnormal splice variant in the WT/mt and mt/mt medaka (Fig. 4C), and the sequence of these PCR products indicated that exon 13 was skipped in the mutant mRNAs (Fig. 4D). Surprisingly, this abnormal splicing pattern was almost identical to that in the human KRS/PARK9 patient [3], in which the 111-bp exon 13 is skipped (Fig. S4B). Real-time PCR showed a marked reduction (17.8%) in the normal *atp13a2* mRNA in the mt/mt medaka brain (Fig. 4E). We therefore concluded that we had succeeded in identifying an Atp13a2 mutant in medaka, and this mutation was similar to a pathogenic KRS/PARK9 mutation in human.

Atp13a2 mutant medaka fish grew normally during early development without any obvious morphological abnormalities.

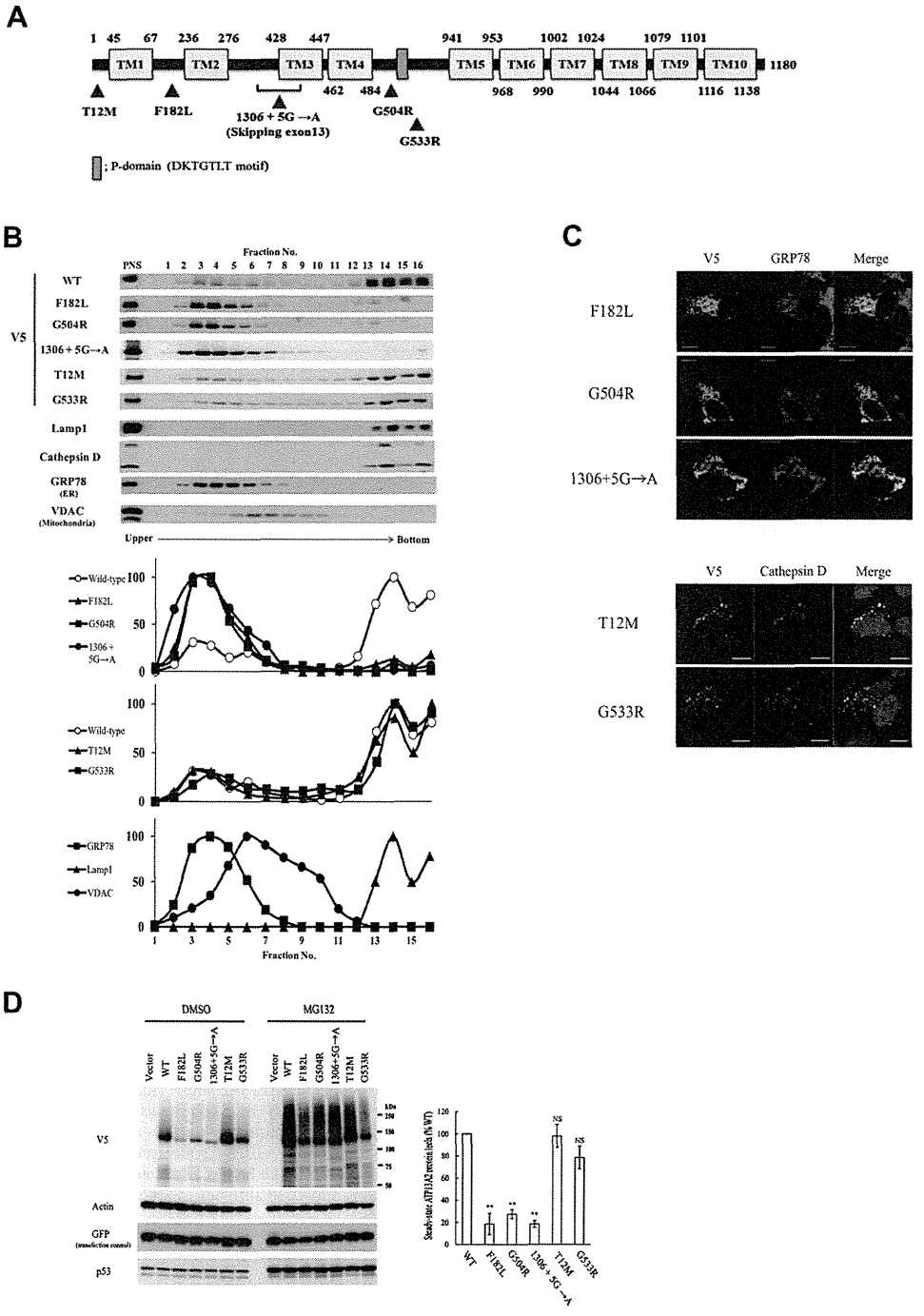

Fig. 2. Characterization of subcellular localization of KRS mutants. (A) Schematic diagram of disease-relevant mutants of ATP13A2 used in this study. (B) Percoll gradient fractionation of ATP13A2 protein. The graphs indicate densitometry of bands. This Percoll gradient system separates dense lysosomes (near bottom, Fraction 13–16) from lighter particles such as ER (Fraction 2–8). (C) Double immunofluorescence studies for KRS mutants. Colocalization of T12M or G533R with cathepsin D, a lysosomal protein, is observed. Other mutants localizes with GRP78, a resident ER chaperone protein. (D) Protein blot analysis of ATP13A2 WT and mutant V5-tagged constructs in transiently transfected SH-SY5Y cells. GFP was co-transfected with the ATP13A2s as a transfection control. The proteasome inhibitor MG132 (10 μM) stabilizes PARK9 mutants after 24 h. The antibody against p53, whose degradation is known to dependent to proteasome, is used as a control for MG132 treatment. Densitometry analysis indicates the steady state protein levels of each variant. Data are represented as percent of WT. Error bars, S.E.M. $n = 3$. $^{**}P < 0.01$ vs WT.

Remarkably, the mt/mt medaka fish showed a significant reduction of the life span relative to WT/WT and to WT/mt fish (Fig. 4F). The body weight of mt/mt fish was normal (Fig. 4G). We examined the internal organs including brains of the dead mt/mt fish, but we could not identify a specific reason for the shorter lifespan of mt/mt medaka fish. We next quantified spontaneous swimming movement in mt/mt medaka fish. At 4 months, mt/mt fish exhibited a mild locomotor increase with significant differences reported only in swimming duration whereas distance and velocity are normal. All the genotypes showed comparable movement at 12 months, irrespective of *atp13a2* genotype (Fig. 4H).

Collectively, we generated *atp13a2* mutant medaka fish carrying almost identical mutation to human KRS/PARK9 patient. The homozygous mutant fish grew normally, but relative to wild-type and heterozygous animals, these mutants exhibited more spontaneous swimming movement at 4 months and had a shorter life span.

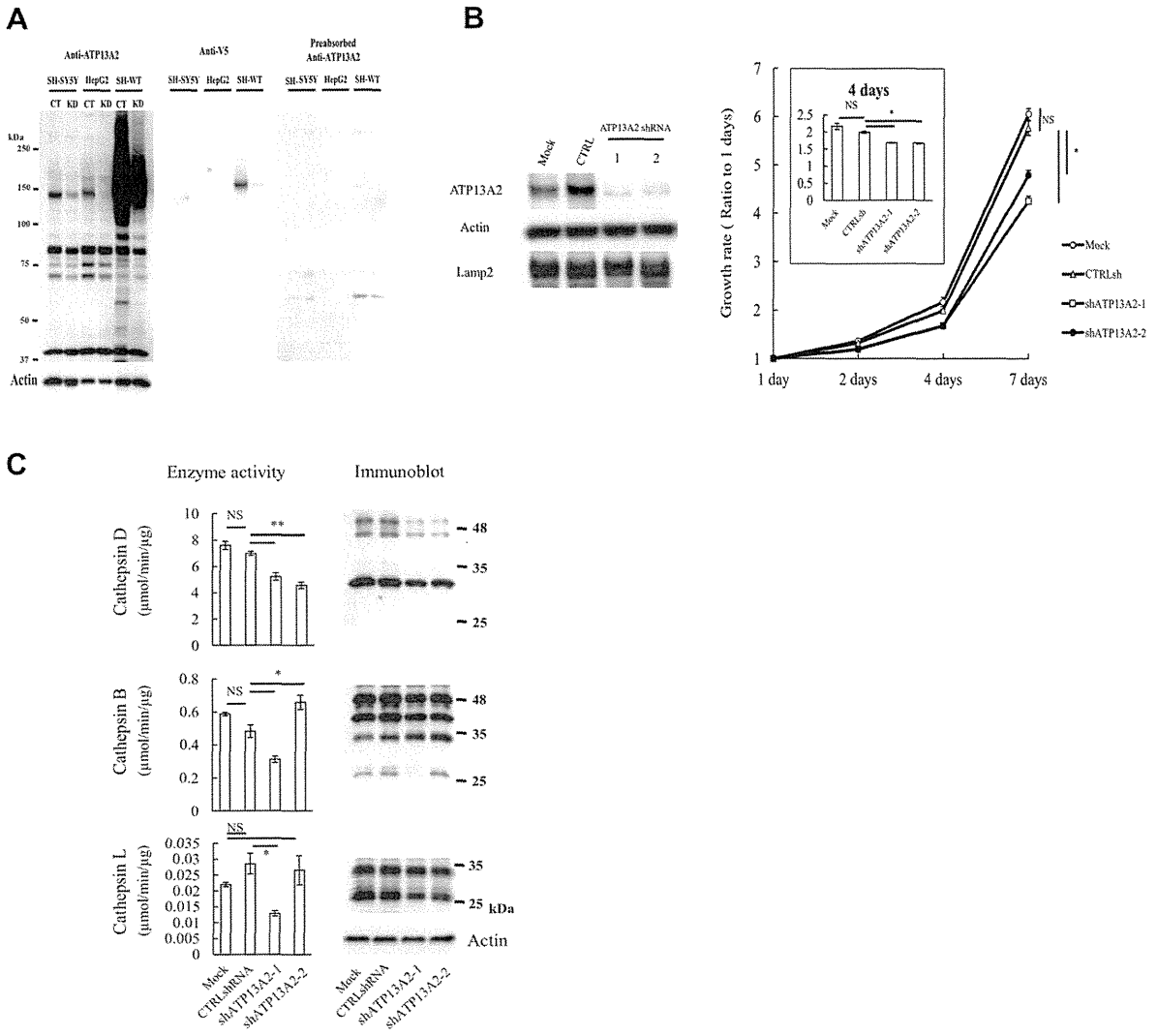

Fig. 3. Suppression of ATP13A2 leads to cathepsin D deficiency and accumulation of fingerprint-like structures in SH-SY5Y cells. (A) Immunoblotting with anti-ATP13A2 antibody (left panel), anti-V5 antibody (middle panel) and anti-ATP13A2 antibody (preabsorbed) (right panel) shows the ATP13A2 expression levels of SH-SY5Y cells, HepG2 cells and SH-SY5Y cells stably expressing WT (SH-WT). Cells are transfected with negative control (CT) or ATP13A2 siRNA (KD) for 72 h. (B) Immunoblotting using anti-ATP13A2 antibody and cell growth assay of SH-SY5Y cell lines stably expressing shRNA against human ATP13A2. The graph shows the growth rate of cells. Data are the means of triplicate experiments. Error bars, S.E.M. $^{*}P < 0.05$. (C) Measurement of cathepsin D, B and L activity and protein level in the extracts from ATP13A2-knockdown SH-SY5Y cells. Enzyme activity assays were performed in three independent experiments. Error bars, S.E.M. $^{*}P < 0.05$. $^{**}P < 0.01$. (D) Electron microscopic examination of SH-SY5Y cells that stably express shATP13A2-1 or shATP13A2-2. The diminished ATP13A2 expression induces lysosome-like bodies that contain granular deposits and fingerprint-like structure. Boxed areas (d) are shown enlarged in the left (e). (E) Evaluation of LC3 accumulation using anti-LC3B antibody in SH-SY5Y cell lines stably expressing shATP13A2 (each 3 clones). $^{**}P < 0.01$.

2.4. Neuropathology of Atp13a2 mutant medaka fish

Selective and progressive loss of dopaminergic/noradrenergic cells constitutes the characteristic pathology of human PD patients. Having previously identified TH-positive (TH+) dopaminergic neurons and noradrenergic neurons in the medaka brain [17], we could examine histologically these TH+ neurons in the brain tissue of *atp13a2* mutants. At 4 months, the number of TH+ neurons did not differ significantly among mt/mt, mt/WT, and WT/WT fish. However at 8 and 12 months, the number of TH+ neurons in the middle diencephalon and the density of TH+ fibers in the telencephalon were lower in the mt/mt medaka than in mt/WT or in WT/WT fish (Fig. 5A). The mt/mt medaka fish at these stages also had fewer noradrenergic neurons in the medulla oblongata than did mt/WT or WT/WT fish (Fig. 5A). The reduction of TH+ neurons was not robust but age-dependent and progressive. Additionally, we examined tryptophan hydroxylase and serotonin levels via immunohistochemistry; neither the number of tryptophan hydroxylase positive neurons in the raphe nor the intensity of serotonin signals in the diencephalon differed significantly among all the genotypes (Fig. 5A). Although no TUNEL-positive dopaminergic neuron was observed in the WT/WT brains, a few TUNEL/TH double positive neurons were detected in the mt/mt brains (Fig. 5B). To exclude the possibility of developmental disorder of the dopaminergic neurons, we also counted the TH+ neurons in the middle diencephalon at 1 month. At this larval stage, mt/mt fish showed comparable number of dopaminergic neurons to WT/WT fish (Fig. S5) indicating the loss of dopaminergic neurons seen at 8 and 12 months was indeed late-onset phenotype. Next, we measured the amount of dopamine, noradrenaline, and serotonin in whole-brain samples from mutant fish at 4 and 12 months. The amount of dopamine in the brain samples from mt/mt medaka

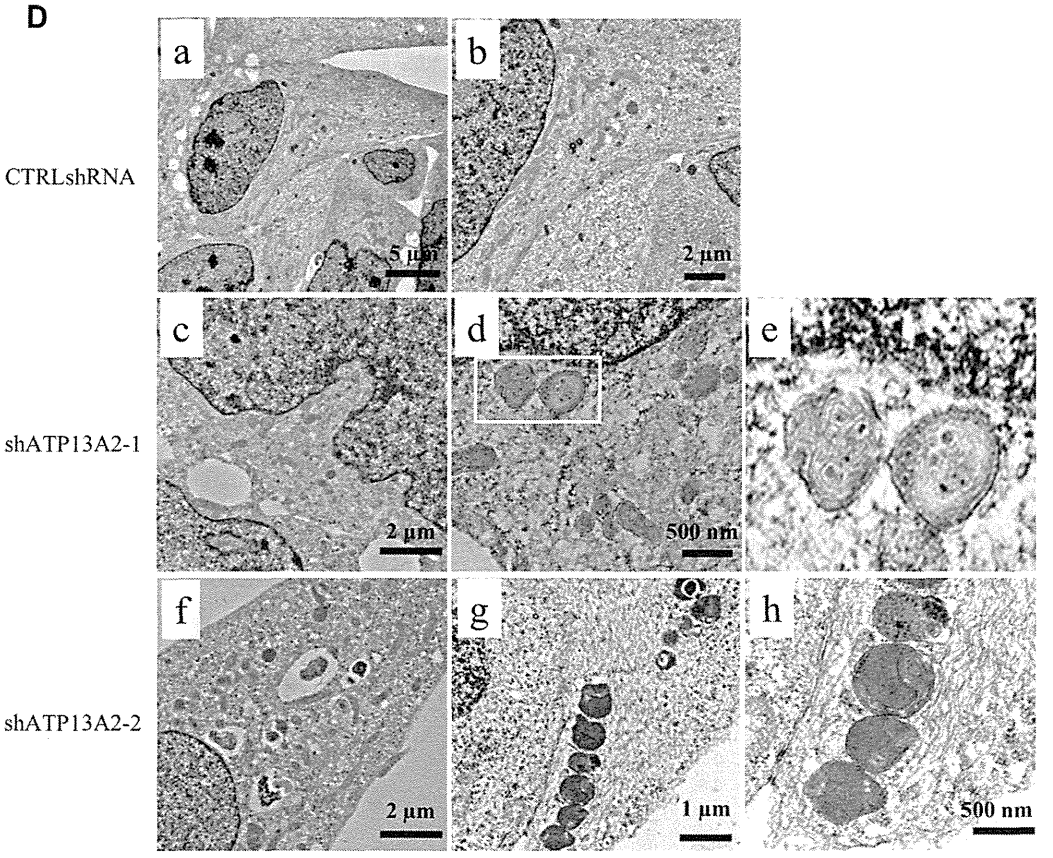

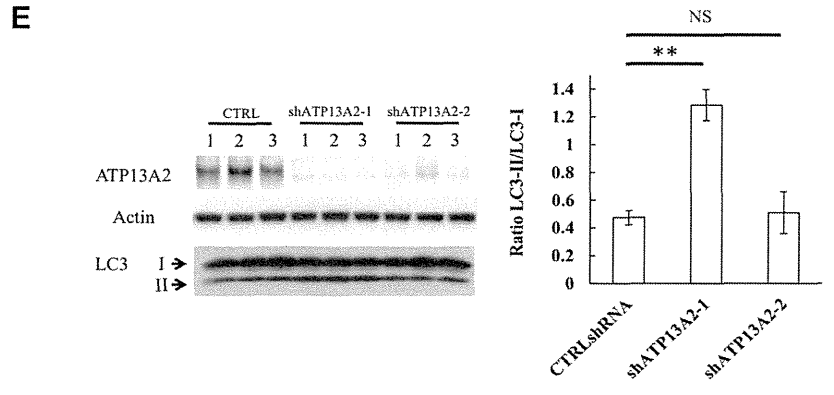

Fig. 3. (*continued*)

was comparable to that in the WT/WT or the WT/mt at 4 months, but lower than that in the WT/WT or the WT/mt at 12 months (Fig. 5C, upper). The noradrenaline in mt/mt medaka brain samples also tended to be lower at 12 months, but the differences were not statistically significant (Fig. 5C, middle). The amount of serotonin in whole-brain samples did not differ significantly among the genotypes (Fig. 5C, lower). Taken together, these findings indicated that *atp13a2* homozygous mutant medaka fish showed selective and progressive loss of dopaminergic/noradrenergic neurons, and such loss is a typical feature of human PD.

To examine in further detail the pathology associated with the *apt13a2* mutation, middle diencephalon samples from mt/mt, mt/WT, and WT/WT animals were analyzed via transmission electron microscopy as described previously [18]. Structures resembling fingerprints-profile, like those seen in ATP13A2-knockdown SH-SY5Y cells, were observed in thin sections taken from each mt/mt brain examined (Fig. 5D). However, these structures were not observed in the sections taken from WT/WT or WT/mt medaka brain samples. Fingerprint-profiles have been observed in cathepsin D-deficient mice [15] and in human patients with neuronal ceroid lipofuscinosis [19–21], and these structures are thought to indicate an autophagy/lysosome disorder. We used western blots to measure the amount of cathepsin D protein in brain tissue samples, and we found that mt/mt fish had less cathepsin D protein than did mt/WT or WT/WT fish (Fig. 5E and S6). We also showed that mt/mt medaka brain tissue, like the ATP13A2-knockdown cells, exhibited a significant reduction in cathepsin D activity (Fig. 5E). However, cathepsin K activity, cathepsin H activity, and proteasome activity were not affected by the *atp13a2* mutation (Fig. 5E), indicating the dysfunction of lysosomal enzymes was relatively specific to cathepsin D. Alpha-synuclein accumulation is one of the specific characters of idiopathic PD patients, Thus, we

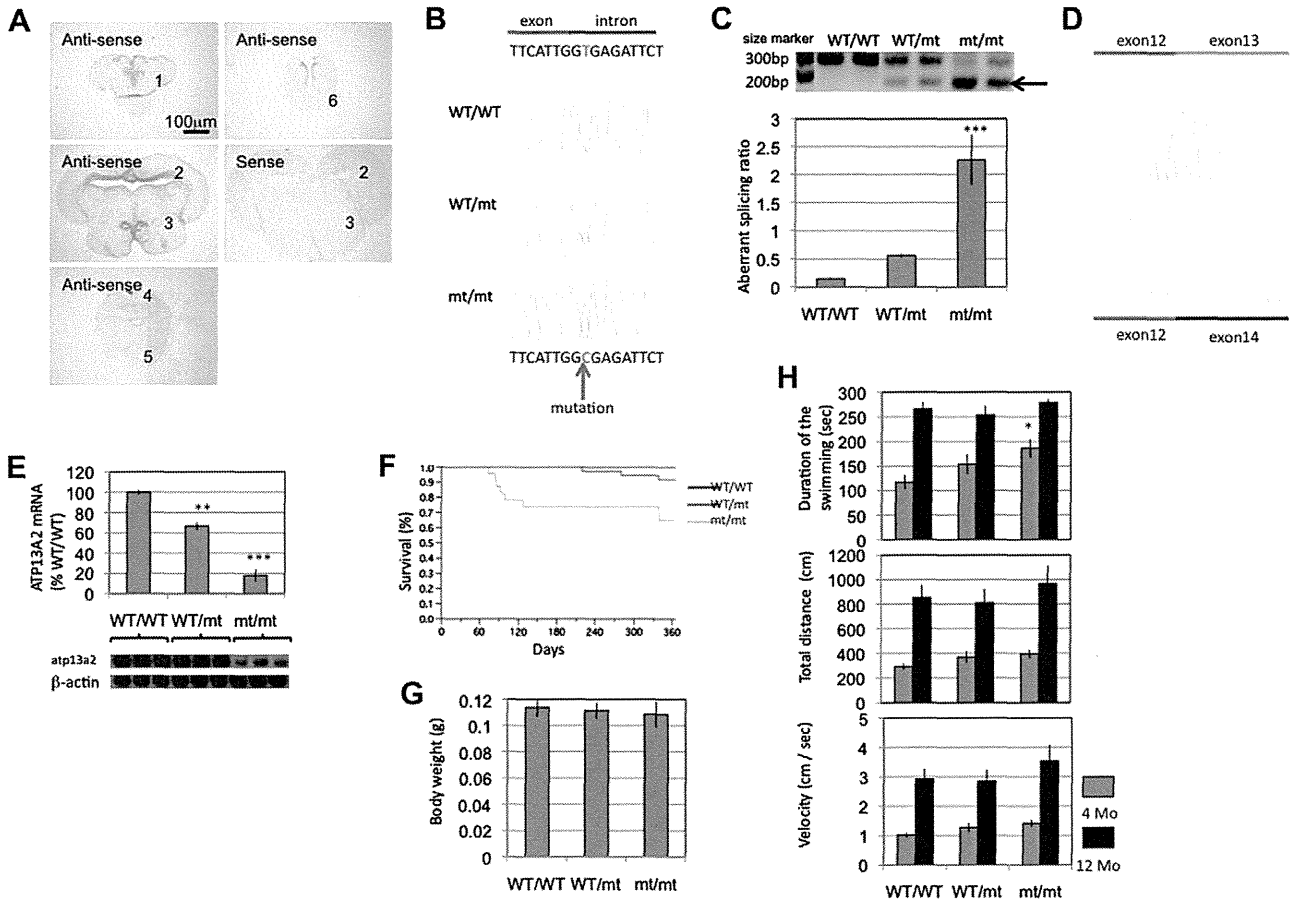

Fig. 4. Generation of Atp13a2 mutant medaka. (A) In situ hybridization of medaka *atp13a2* mRNA. Anti-sense signals and sense control of *Kyoto-Cab* medaka brain (12 months). 1: telencephalon, 2: optic tectum, 3: diencephalon, 4: cerebellum, 5: medulla oblongata, 6: spinal cord. (B) Sequence data for each genotype. A = green, T = red, G = black, and C = blue. The red arrow indicates the mutation site. This T to C mutation in the genomic sequence disrupts a splice donor site. (C) RT-PCR amplification of *atp13a2* mRNA from each genotype. WT/WT medaka show single band, whereas WT/mt and mt/mt medaka have an additional shorter band (arrow). bp: Base pairs. The graph indicates densitometric ratio of the shorter product/normal product. ***$P < 0.001$ vs. WT/WT and $P < 0.01$ vs. WT/mt. $n = 4$ for each genotype. Error bars, S.E.M. (D) Sequence of the PCR products. The upper band indicates the normal splicing product and the lower band is the abnormal splicing product. Exon 13 skipping occurrs in the Atp13a2 mutant medaka. (E) Real-time PCR of normal *atp13a2* mRNA. **: $P < 0.01$ vs. WT/WT, ***: $P < 0.001$ vs. WT/WT and WT/mt. $n = 3$ for each genotype. Error bars, S.E.M. (F) Survival curves of each genotype. The end point is the death of each medaka or day 365. The results show mild but significant shortening of the life span in mt/mt medaka ($P < 0.001$) ($n = 23$), relative to that in WT/WT ($n = 25$) or WT/mt ($n = 37$). Death before 1 month stage was not counted. (G) Body weight of Atp13a2 mutant medaka at 12 months. No significant differences were seen ($n = 20$ for each group). Error bars, S.E.M. (H) Duration of swimming, total swimming distance and swimming velocity during spontaneous swimming behavior of Atp13a2 mutant medaka ($n = 15$ for each group). *$P < 0.05$ vs. WT/WT. Error bars, S.E.M.

analyzed the alpha-synuclein status in our cell line and medaka models. However, we could not demonstrate consistent and significant differences between ATP13A2-deficient models and controls (Figs. S3 and S7), and these findings indicated that alpha-synuclein accumulation might not be the causative roles of KRS/PARK9.

In sum, *atp13a2* homozygous mutant medaka exhibited dopaminergic neurodegeneration, a deficiency of cathepsin D, and abnormal lysosome-related structures in the brain.

3. Discussion

Findings from previous studies clearly indicate that PARK gene products associate with each other via protein degradation pathways including the autophagy–lysosome system. Indeed, dysfunction of protein degradation has emerged as an important contributor to nigral neuronal death in PD. Presence of Lewy bodies is strong evidence of impaired protein degradation in PD. Lewy bodies consist of aggregated proteins, and alpha-synuclein is a major component of these structures [22]. Thus aggregation of alpha-synuclein has emerged as one of the most important processes in nigral degeneration in PD. Although soluble alpha-synuclein is degraded both during autophagy and by the proteasome, aggregated alpha-synuclein is degraded and cleared mainly via the autophagy–lysosome pathway [23]. Other PARK gene products, specifically Parkin and PINK1, work together to clear damaged mitochondria from cells via mitochondria-specific autophagy called mitophagy [24]. Furthermore, ATP13A2 mainly localizes to lysosomes, as we and other groups demonstrated [3,10–14,25]. Recently, mutations in the gene encoding glucocerebrosidase (GBA), a lysosomal enzyme, have been shown to be significant genetic risk factors for PD [26]. These observations indicate that lysosomal function is important for the maintenance of dopamine neurons, and they led us to investigate the function of ATP13A2 in the pathophysiology of KRS/PARK9.

ATP13A2 deficiency resulted in an abnormal aggregation of lysosomes at perinuclear site. Furthermore, these accumulated vesicles were enlarged, as previously reported [27]. Moreover, we found evidence of lysosomal dysfunction in that cathepsin D activity was, specifically, reduced in ATP13A2-knockdown cells. Cathepsin D is a ubiquitously expressed lysosomal protease that is involved in proteolytic degradation, cell invasion, and apoptosis. Cathepsin D deficiencies cause neuronal ceroid lipofuscinosis, a

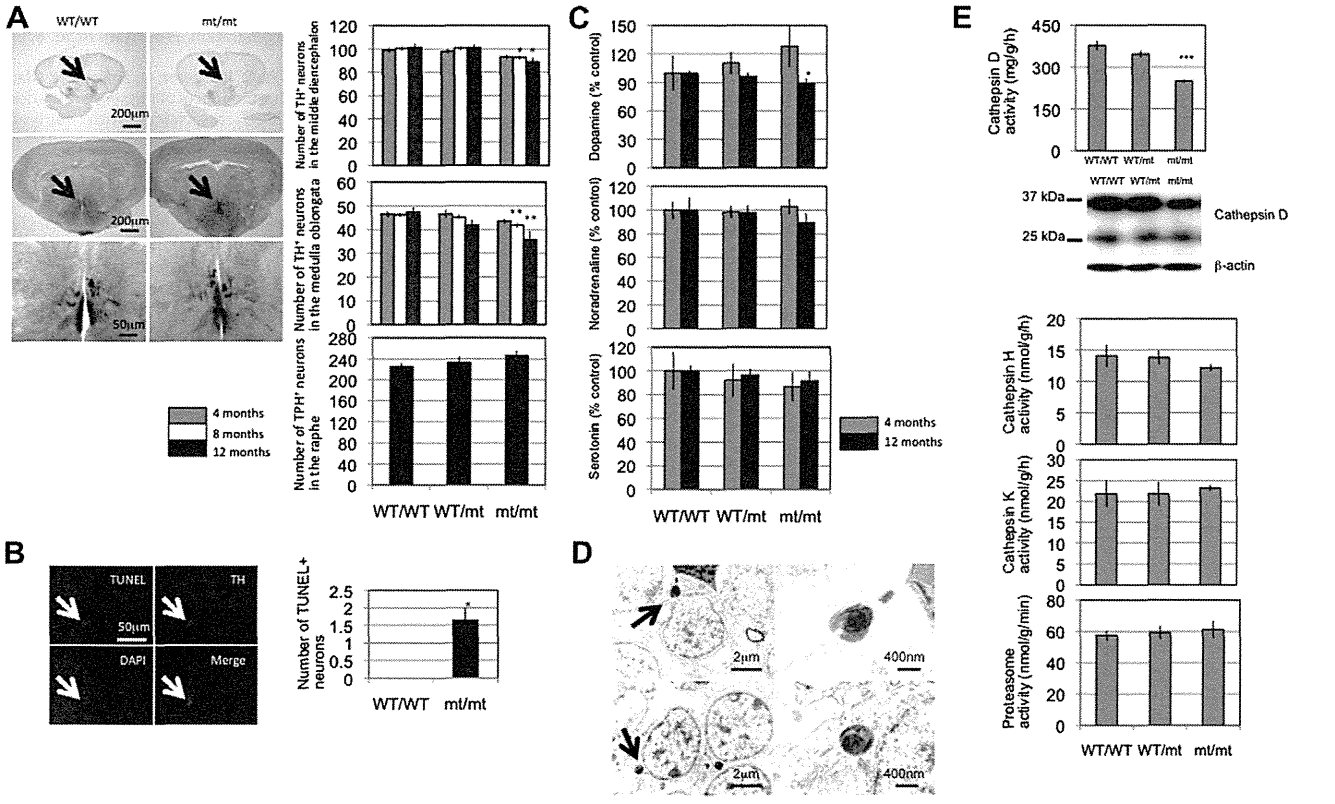

Fig. 5. Neuropathology of Atp13a2 mutant medaka. (A) Axial sections of telencephalon (upper) and middle diencephalon (middle and lower) of medaka brain at 12 months. Arrows indicate TH+ fibers and neurons. The lower figures are the enlarged image of middle figures. The graphs indicate the number of TH+ neurons in the middle diencephalon (upper) and medulla oblongata (middle) and the number of tryptophan-hydroxylase positive (TPH+) neurons in the raphe. $^{*}P < 0.05$ vs. WT/WT and WT/mt. $^{**}P < 0.01$ vs. WT/WT. ($n = 16$ for each group). Error bars, SEM. (B) TUNEL assay in medaka brain at 12 months. White arrow indicates one TUNEL/TH double positive neuron in the middle diencephalon of mt/mt fish. The graph shows the number of TH/TUNEL double positive neurons in the middle diencephalon ($n = 3$). $^{*}P < 0.05$ vs. WT/WT. (C) Amount of dopamine (upper), noradrenaline (middle), and serotonin (lower) in the brain of Atp13a2 mutant medaka. All values are expressed as a percentage of the amount (ng) per protein weight (mg) for WT/WT ($n = 8$ for each group). $^{*}P < 0.05$ vs. WT/WT. Error bars, S.E.M. (D) Fingerprint-like structures in Atp13a2 mutant medaka brain. Arrows indicate fingerprint-like structures in mt/mt brain. The right figures are the high magnification images of these structures. (E) Enzyme activity (Cathepsin D, H, K and proteasome activity) in the medaka brain. $^{***}P < 0.001$ vs. WT/T and WT/mt. Error bars, SEM. Image of a western blot shows cathepsin D protein in the medaka brain. Cross reactivity of the antibody against medaka cathepsin D is shown in the supplementary information (Fig. S5).

fatal neurogenerative disease in human and sheep [21,28–30]. Using electronmicroscopy, we also detected lysosome like body and granular deposits. Interestingly, we observed subcellular structures that resemble fingerprint-profile, and these structures resemble abnormal structures in the neurons of cathepsin D-deficient mice [15] and in human patients with neuronal ceroid lipofuscinosis [19–21] or with sphingolipidoses [31,32]. These results indicate that the primary cause of KRS/PARK9 is a lysosomal dysfunction and KRS/PARK9 could also be classified into a "lysosome disease".

We have recently used medaka fish to develop an animal model of PD [17,18,33,34]. Here, we found a mutation in our TILLING library that is almost identical to a PD-associated mutation in human patients. This medaka mutation results in the same abnormal splicing that is seen in the human patients with KRS/PARK9. Homozygous mutant fish exhibited selective loss of dopaminergic and noradrenergic neurons; this type of neuron loss is a pathology typically seen in human PD patients. Additionally, we found that tissues and cells in the brains from homozygous mutant medaka exhibited a specific reduction of cathepsin D protein and developed fingerprint-like subcellular structures. Both findings strongly indicate that the ATP13A2 mutation could lead to the dysfunction of lysosomes in medaka neurons.

Recently, Fonseca et al. injected Morpholinos against *atp13a2* into zebrafish embryo and showed that loss of Atp13a2 results in embryonic lethality [35]. As they also showed in zebrafish, *atp13a2* mRNA expressed not only in the brain but also in the entire body in medaka larvae (data not shown). This suggested that Atp13a2 is also important for some unknown function in other organs than the central nervous system. Our medaka model mimics the human mutation and showed pronounced reduction of *atp13a2* mRNA but not null expression. This might be helpful to study the long-term effect of Atp13a2 dysfunction.

As is the case of human patients with PD, cell death was specific to dopamine and noradrenaline neurons in our medaka model of KRS/ATP13A2. This cell-type specificity is also evident with our other medaka models of PD, including the models resulting from a lysosome inhibitor treatment [18,34]. The *atp13a2* mRNA, like other PD-related mRNAs, is expressed ubiquitously in the medaka brain [33]. Thus, the expression pattern of *atp13a2* could not explain the selective cell death in our model. Dopamine neurons contain toxic proteins derived from dopamine itself [36,37], and lysosomal function is essential in these neurons for preventing accumulation of the toxic proteins and other toxic metabolic products. Therefore, we speculate that dopamine neurons are especially vulnerable to lysosome dysfunction.

One negative finding is that mutant fish did not show slow locomotive movement, as do human PD patients. Based on our analysis, it seemed that the mutant fish swam the same amount, or more, than did control fish. In humans, loss of at least 80% of the dopaminergic neurons in substantia nigra seems necessary to evoke clear PD symptoms. The extent of the loss of dopaminergic

neurons in our medaka model might not be enough to evoke locomotive impairment. The mild increase of locomotion at 4 months seen in homozygous mutant might have a relation with the non-significant increase of dopamine at the same stage. Similar tentative increase of dopamine at younger stage is also observed in another PD model fish [33]. Such increased dopamine might harm the neurons, because the metabolism of dopamine is accompanied by the generation of oxidative radicals [38].

In conclusion, we demonstrated that reduction in ATP13A2 function in vitro or in vivo resulted in dysfunction of cathepsin D and the appearance of abnormal structures that are associated with lysosomal disorders. We used a teleost fish, medaka, to successfully generate an animal model suffered selective degeneration of dopaminergic neurons. Our findings indicate that lysosome-mediated autophagy may play a key role to protect dopaminergic neurons.

Acknowledgments

We wish to thank Kondoh Differentiation Signaling Project, JST, for permission to use the Kyoto-cab strain. We are grateful to Ai Tanigaki, Rie Hikawa and Junji Ezaki, who were very supportive of our experiments. We are also grateful to Satoshi Fukui, Mitsutaka Yoshida, Kaori Moriya, and Hidetake Kurihara for excellent assistance with our electron microscopy studies. This work was supported by JST-CREST. A part of this research was supported by a Grant-in-Aid for Young Scientists (B) (F. Sato) and a Grant-in-Aid for Scientific Research on Innovative Areas (Comprehensive Brain Science Network) (F. Sato) from the Ministry of Education, Science, Sports and Culture of Japan.

Appendix A. Supplementary data

Supplementary data associated with this article can be found, in the online version, at http://dx.doi.org/10.1016/j.febslet.2013.02.046.

References

[1] Gasser, T. (2007) Update on the genetics of Parkinson's disease. Mov. Disord. 22 (Suppl. 17), S343–S350.
[2] Najim al-Din, A.S., Wriekat, A., Mubaidin, A., Dasouki, M. and Hiari, M. (1994) Pallido-pyramidal degeneration, supranuclear upgaze paresis and dementia: Kufor-Rakeb syndrome. Acta Neurol. Scand. 89, 347–352.
[3] Ramirez, A., Heimbach, A., Gründemann, J., Stiller, B., Hampshire, D., Cid, L.P., Goebel, I., Mubaidin, A.F., Wriekat, A.L., Roeper, J., et al. (2006) Hereditary parkinsonism with dementia is caused by mutations in ATP13A2, encoding a lysosomal type 5 P-type ATPase. Nat. Genet. 38, 1184–1191.
[4] Di Fonzo, A., Chien, H.F., Socal, M., Giraudo, S., Tassorelli, C., Iliceto, G., Fabbrini, G., Marconi, R., Fincati, E., Abbruzzese, G., et al. (2007) ATP13A2 missense mutations in juvenile parkinsonism and young onset Parkinson disease. Neurology 68, 1557–1562.
[5] Ning, Y.P., Kanai, K., Tomiyama, H., Li, Y., Funayama, M., Yoshino, H., Sato, S., Asahina, M., Kuwabara, S., Takeda, A., et al. (2008) PARK9-linked parkinsonism in eastern Asia: mutation detection in ATP13A2 and clinical phenotype. Neurology 70, 1491–1493.
[6] Paisán-Ruiz, C., Guevara, R., Federoff, M., Hanagasi, H., Sina, F., Elahi, E., Schneider, S.A., Schwingenschuh, P., Bajaj, N., Emre, M., et al. (2010) Early-onset L-dopa-responsive parkinsonism with pyramidal signs due to ATP13A2, PLA2G6, FBXO7 and spatacsin mutations. Mov. Disord. 25, 1791–1800.
[7] Santoro, L., Breedveld, G.J., Manganelli, F., Iodice, R., Pisciotta, C., et al. (2011) Novel ATP13A2 (PARK9) homozygous mutation in a family with marked phenotype variability. Neurogenetics 12, 33–39.
[8] Crosiers, D., Ceulemans, B., Meeus, B., Nuytemans, K., Pals, P., Van Broeckhoven, C., Cras, P. and Theuns, J. (2011) Juvenile dystonia–parkinsonism and dementia caused by a novel ATP13A2 frame-shift mutation. Parkinsonism Relat. Disord. 17, 135–138.
[9] Lesage, S. and Brice, A. (2009) Parkinson's disease: from monogenic forms to genetic susceptibility factors. Hum. Mol. Genet. 18, R48–R59.
[10] Covy, J.P., Waxman, E.A. and Giasson, B.I. (2012) Characterization of cellular protective effects of ATP13A2/PARK9 expression and alterations resulting from pathogenic mutants. J. Neurosci. Res. 90, 2306–2316.
[11] Dehay, B., Ramirez, A., Martinez-Vicente, M., Perier, C., Canron, M.H., Doudnikoff, E., Vital, A., Vila, M., Klein, C. and Bezard, E.C. (2012) Loss of P-type ATPase ATP13A2/PARK9 function induces general lysosomal deficiency and leads to Parkinson disease neurodegeneration. Proc. Natl. Acad. Sci. USA 109, 9611–9616.
[12] Podhajska, A., Musso, A., Trancikova, A., Stafa, K., Moser, R., Sonnay, S., Glauser, L. and Moore, D.J. (2012) Common pathogenic effects of missense mutations in the P-type ATPase ATP13A2 (PARK9) associated with early-onset parkinsonism. PLoS ONE 7, e39942.
[13] Ramonet, D., Podhajska, A., Stafa, K., Sonnay, S., Trancikova, A., Tsika, E., Pletnikova, O., Troncoso, J.C., Glauser, L. and Moore, D.J. (2012) PARK9-associated ATP13A2 localizes to intracellular acidic vesicles and regulates cation homeostasis and neuronal integrity. Hum. Mol. Genet. 21, 1725–1743.
[14] Usenovic, M., Knight, A.L., Ray, A., Wong, V., Brown, K.R., Caldwell, G.A., Caldwell, K.A., Stagljar, I. and Krainc, D. (2012) Identification of novel ATP13A2 interactors and their role in α-synuclein misfolding and toxicity. Hum. Mol. Genet. 21, 3785–3794.
[15] Koike, M., Nakanishi, H., Saftig, P., Ezaki, J., Isahara, K., Ohsawa, Y., Schulz-Schaeffer, W., Watanabe, T., Waguri, S., Kametaka, S., et al. (2000) Cathepsin D deficiency induces lysosomal storage with ceroid lipofuscin in mouse CNS neurons. J. Neurosci. 20, 6898–6906.
[16] Taniguchi, Y., Takeda, S., Furutani-Seiki, M., Kamei, Y., Todo, T., Sasado, T., Deguchi, T., Kondoh, H., Mudde, J., Yamazoe, M., et al. (2006) Generation of medaka gene knockout models by target-selected mutagenesis. Genome Biol. 7, R116.
[17] Matsui, H., Taniguchi, Y., Inoue, H., Uemura, K., Takeda, S. and Takahashi, R. (2009) A chemical neurotoxin, MPTP induces Parkinson's disease like phenotype, movement disorders and persistent loss of dopamine neurons in medaka fish. Neurosci. Res. 65, 263–271.
[18] Matsui, H., Ito, H., Taniguchi, Y., Inoue, H., Takeda, S. and Takahashi, R. (2010) Proteasome inhibition in medaka brain induces the features of Parkinson's disease. J. Neurochem. 115, 178–187.
[19] Palmer, D.N., Fearnley, I.M., Walker, J.E., Hall, N.A., Lake, B.D., Wolfe, L.S., Haltia, M., Martinus, R.D. and Jolly, R.D. (1992) Mitochondrial ATP synthase subunit c storage in the ceroid-lipofuscinoses (Batten disease). Am. J. Med. Genet. 42, 561–567.
[20] Tsiakas, K., Steinfeld, R., Storch, S., Ezaki, J., Lukacs, Z., Kominami, E., Kohlschütter, A., Ullrich, K. and Braulke, T. (2004) Mutation of the glycosylated asparagine residue 286 in human CLN2 protein results in loss of enzymatic activity. Glycobiology 14, 1C–5C.
[21] Tyynelä, J., Palmer, D.N., Baumann, M. and Haltia, M. (1993) Storage of saposins A and D in infantile neuronal ceroid-lipofuscinosis. FEBS Lett. 330, 8–12.
[22] Spillantini, M.G., Schmidt, M.L., Lee, V.M., Trojanowski, J.Q., Jakes, R. and Goedert, M. (1997) Alpha-synuclein in Lewy bodies. Nature 388, 839–840.
[23] Webb, J.L., Ravikumar, B., Atkins, J., Skepper, J.N. and Rubinsztein, D.C. (2003) Alpha-synuclein is degraded by both autophagy and the proteasome. J. Biol. Chem. 278, 25009–25013.
[24] Narendra, D., Tanaka, A., Suen, D.F. and Youle, R.J. (2008) Parkin is recruited selectively to impaired mitochondria and promotes their autophagy. J. Cell Biol. 183, 795–803.
[25] Tan, J., Zhang, T., Jiang, L., Chi, J., Hu, D., Pan, Q., Wang, D. and Zhang, Z. (2011) Regulation of intracellular manganese homeostasis by Kufor-Rakeb syndrome-associated ATP13A2 protein. J. Biol. Chem. 286, 29654–29662.
[26] Sidransky, E., Nalls, M.A., Aasly, J.O., Aharon-Peretz, J., Annesi, G., Barbosa, E.R., Bar-Shira, A., Berg, D., Bras, J., Brice, A., et al. (2009) Multicenter analysis of glucocerebrosidase mutations in Parkinson's disease. N. Engl. J. Med. 361, 1651–1661.
[27] Usenovic, M., Tresse, E., Mazzulli, J.R., Taylor, J.P. and Krainc, D. (2012) Deficiency of ATP13A2 leads to lysosomal dysfunction, α-synuclein accumulation, and neurotoxicity. J. Neurosci. 32, 4240–4246.
[28] Siintola, E., Partanen, S., Strömme, P., Haapanen, A., Haltia, M., Maehlen, J., Lehesjoki, A.E. and Tyynelä, J. (2006) Cathepsin D deficiency underlies congenital human neuronal ceroid-lipofuscinosis. Brain 129, 1438–1445.
[29] Fritchie, K., Siintola, E., Armao, D., Lehesjoki, A.E., Marino, T., Powell, C., Tennison, M., Booker, J.M., Koch, S., Partanen, S., et al. (2009) Novel mutation and the first prenatal screening of cathepsin D deficiency (CLN10). Acta Neuropathol. 117, 201–208.
[30] Steinfeld, R., Reinhardt, K., Schreiber, K., Hillebrand, M., Kraetzner, R., Bruck, W., Saftig, P. and Gartner, J. (2006) Cathepsin D deficiency is associated with a human neurodegenerative disorder. Am. J. Hum. Genet. 78, 988–998.
[31] Jellinger, K., Anzil, A.P., Seemann, D. and Bernheimer, H. (1982) Adult GM2 gangliosidosis masquerading as slowly progressive muscular atrophy: motor neuron disease phenotype. Clin. Neuropathol. 1, 31–44.
[32] Idoate, M.A., Pardo-Mindan, F.J. and Gonzalez Alamillo, C. (1992) Fabry's disease without angiokeratomas showing unusual eccrine gland vacuolation. J. Pathol. 167, 65–68.
[33] Matsui, H., Taniguchi, Y., Inoue, H., Kobayashi, Y., Sakaki, Y., Toyoda, A., Uemura, K., Kobayashi, D., Takeda, S. and Takahashi, R. (2010) Loss of PINK1 in medaka fish (*Oryzias latipes*) causes late-onset decrease in spontaneous movement. Neurosci. Res. 66, 151–161.
[34] Matsui, H., Ito, H., Taniguchi, Y., Takeda, S. and Takahashi, R. (2010) Ammonium chloride and tunicamycin are novel toxins for dopaminergic neurons and induce Parkinson's disease-like phenotypes in medaka fish. J. Neurochem. 115, 1150–1160.

[35] Lopes da Fonseca, T., Correia, A., Hasselaar, W., van der Linde, H.C., Willemsen, R. and Outeiro, T.F. (2013) The zebrafish homologue of Parkinson's disease ATP13A2 is essential for embryonic survival. Brain Res. Bull. 90, 118–126.
[36] Barzilai, A., Daily, D., Zilkha-Falb, R., Ziv, I., Offen, D., Melamed, E. and Shirvan, A. (2003) The molecular mechanisms of dopamine toxicity. Adv. Neurol. 91, 73–82.
[37] Gandhi, S., Vaarmann, A., Yao, Z., Duchen, M.R., Wood, N.W. and Abramov, A.Y. (2012) Dopamine induced neurodegeneration in a PINK1 model of Parkinson's disease. PLoS ONE 7, e37564.
[38] Blum, D., Torch, S., Lambeng, N., Nissou, M., Benabid, A.L., Sadoul, R. and Verna, J.M. (2001) Molecular pathways involved in the neurotoxicity of 6-OHDA, dopamine and MPTP: contribution to the apoptotic theory in Parkinson's disease. Prog. Neurobiol. 65, 135–172.

Neurobiology of Aging 35 (2014) 935.e3–935.e8

Contents lists available at ScienceDirect

Neurobiology of Aging

journal homepage: www.elsevier.com/locate/neuaging

Brief communication

Clinicogenetic study of *GBA* mutations in patients with familial Parkinson's disease

Yuanzhe Li [a,b], Takeshi Sekine [b], Manabu Funayama [a,b], Lin Li [b], Hiroyo Yoshino [a], Kenya Nishioka [b], Hiroyuki Tomiyama [b,c], Nobutaka Hattori [a,b,c,*]

[a] *Research Institute for Diseases of Old Age, Juntendo University School of Medicine, Tokyo, Japan*
[b] *Department of Neurology, Juntendo University School of Medicine, Tokyo, Japan*
[c] *Department of Neuroscience for Neurodegenerative Disorders, Juntendo University School of Medicine, Tokyo, Japan*

ARTICLE INFO

Article history:
Received 13 May 2013
Received in revised form 11 September 2013
Accepted 12 September 2013
Available online 12 October 2013

Keywords:
Parkinson's disease/Parkinsonism
GBA
Dementia
Gaucher disease

ABSTRACT

The glucocerebrosidase gene (*GBA*) is a known risk factor of Parkinson's disease (PD). We sequenced entire coding exons and exon/intron boundaries of *GBA* in 147 Japanese familial PD (FPD) patients from 144 families and 100 unrelated control subjects. Twenty-seven of 144 (18.8%) of index patients were heterozygous for known Gaucher disease mutations, suggesting that *GBA* heterozygous mutations are strongly associated with FPD (odds ratio = 22.9, 95% confidence interval = 3.1–171.2). The frequency was significantly higher in autosomal dominant PD (ADPD) compared with autosomal recessive PD. According to clinical assessments, PD patients with *GBA* mutations exhibited typical manifestations of PD or dementia with Lewy bodies (DLB), such as L-dopa responsive parkinsonism with psychiatric problems and/or cognitive decline. Interestingly, they also presented with reduced myocardial ^{123}I-meta-iodobenzylguanidine uptake. Our findings suggest that heterozygous *GBA* mutations are strong risk factors in FPD, especially for autosomal dominant PD. Some patients with *GBA* heterozygous mutations develop clinical features of DLB. We speculate that *GBA* dysfunction may promote Lewy body formation, resulting in more severe PD or DLB phenotypes that are inherited in families.

1. Introduction

Parkinson's disease (PD) is one of the most common neurodegenerative disorders. Patients develop disabled movement and complicating nonmotor symptoms, such as psychiatric disorders, cognitive dysfunction, olfactory nerve dysfunction, and sleep disorders (Weintraub and Burn, 2011). Cardinal features of PD are caused by marked loss of dopaminergic neurons in the substantia nigra, which is evidenced by the pathologic hallmark of Lewy bodies; however, PD is a more complicated and systemic disease. PD etiology was thought to be influenced mainly by the interactions between genetic and environmental factors. Nevertheless, recent developments in genetics have revealed that causative genes are involved in Mendelian-inherited parkinsonism (Hatano et al., 2009). Moreover, recent genome-wide association studies have also identified several common loci as genetic risk factors for PD (Hamza et al., 2010; Satake et al., 2009; Simon-Sanchez et al., 2009). During these studies and a subsequent meta-analysis, rare variants of the glucocerebrosidase gene (*GBA*; MIM#606463) have been found as risk factors of sporadic PD (SPD) (Aharon-Peretz et al., 2004; Sidransky et al., 2009). *GBA* is also known as the causative gene of Gaucher disease (GD), which is caused by a loss of function of hydrolytic enzyme activity and is inherited in an autosomal recessive pattern (Hruska et al., 2008; Tsuji et al., 1987).

Some genetic mutations in *GBA* were characterized as strong risk factors for SPD; however, there are few large studies of *GBA* mutations in familial PD (FPD) (Mitsui et al., 2009; Nishioka et al., 2010; Sidransky et al., 2009). Cosegregation was previously reported in a small number of families (Mitsui et al., 2009). One recent study emphasized an association between *GBA* mutations and cognitive impairment in PD (Alcalay et al., 2012).

In this study, we aimed to clarify the role of *GBA* mutations in PD, especially in FPD, by sequencing *GBA* in 147 FPD patients from 144 families and performing a comparative analysis of the clinical phenotype and severity to evaluate the association between *GBA* mutations and FPD.

2. Methods

2.1. Subjects

The study subjects comprised 147 FPD patients from 144 Japanese families and 100 Japanese controls (Table 1). The cohort of

* Corresponding author at: Department of Neurology, Juntendo University School of Medicine, 2-1-1 Hongo, Bunkyo-ku, Tokyo 113-8421, Japan. Tel.: +81 3 5802 1073; fax: +81 3 5800 0547.
E-mail address: nhattori@juntendo.ac.jp (N. Hattori).

0197-4580/$ – see front matter © 2014 Published by Elsevier Inc.
http://dx.doi.org/10.1016/j.neurobiolaging.2013.09.019

Table 1
Patient information

	n	Male/female	AAS (range)	AAO (range)
Patients	147	59/88	60.0 ± 12.8 (21–84)	50.8 ± 13.9 (13–81)
AD	85	35/50	57.7 ± 13.7 (21–84)	48.3 ± 14.2 (13–77)
AR	62	24/38	63.1 ± 10.8 (37–84)	54.3 ± 12.7 (25–81)
Controls	100	47/53	56.8 ± 16.3 (29–87)	

Key: AAO, age at onset; AAS, age at sampling; AD, autosomal dominant; AR, autosomal recessive.

Japanese patients consisted of 85 autosomal dominant PD (ADPD) and 59 autosomal recessive PD (ARPD). For the mode of inheritance to be considered autosomal dominant, there had to be affected family members in at least 2 consecutive generations; for autosomal recessive, we looked for affected siblings in the same generation. After detecting mutations, family members were analyzed to assess cosegregation. DNA samples were provided from various hospitals. Each patient submitted to a neurologic examination performed by expert neurologists and was given a diagnosis of PD on the basis of established criteria (Hughes et al., 1992). Diagnosis of dementia was given by the each clinician based on Mini Mental State Examination score (Folstein et al., 1975). All patients had good response to L-dopa. This study was approved by the ethics review committee of Juntendo University School of Medicine. All subjects provided informed and written consent prior to participation.

2.2. GBA *mutation analysis*

Genomic DNA was extracted from peripheral blood lymphocytes using standard protocols. Polymerase chain reaction was performed using previously reported primers to avoid amplifying the pseudogene (Mitsui et al., 2009). The purified polymerase chain reaction product obtained by ExoSAP IT (GE Healthcare, Salt Lake City, UT, USA) was subsequently used for dideoxy sequencing with BigDye Terminator Chemistry (Applied Biosystems, Foster City, CA, USA). The resulting products were loaded on ABI 310 or 3130 automated DNA sequence analyzers (Applied Biosystems) and analyzed with Sequencing Analysis Software v5.1 (Applied Biosystems). All exons and exon-intron boundaries were analyzed by direct sequencing.

To confirm Rec*Nci*I allele, we used TOPO TA cloning kit (Invitrogen, Carlsbad, CA, USA) for TA cloning and separating alleles. After separating each allele, direct sequencing was performed as described above.

2.3. *Clinical data analysis*

To clarify the clinical features of patients with *GBA* mutations, 19 items (Table 2) concerning prominent PD symptoms were statistically compared between *GBA* mutation–positive and *GBA* mutation–negative groups. Other affected members with *GBA* mutations were also included.

2.4. *Statistical analysis*

Statistical analysis included the t test, Fisher's exact test, odds ratio, and its confidence interval, using GraphPad Prism version 5.0d (GraphPad Prism Software). The Hardy-Weinberg equilibrium test was performed using SNPAlyze v5.1 software (Dynacom, Chiba, Japan). In all statistical analyses, p values ≤ 0.05 were considered statistically significant.

3. Results

3.1. GBA *mutations observed in FPD*

In this study, we only observed heterozygous mutations; no individual had mutations in both alleles. We detected 6 nonsynonymous mutations: p.I(-20)V, p.G64V, p.R120W, p.D409H, p.L444P, and p.I489V; 1 nonsense mutation: p.W393X; 1 synonymous mutation: p.K466K; 1 frame-shift mutation: c.1447-1466delTGins; and 1 recombinant allele (Rec*Nci*I) in the Japanese population (Table 3). Among them, 5 mutations, p.R120W, p.D409H, p.L444P, c.1447-1466delTGins, and Rec*Nci*I, have been reported as causative mutations in GD patients. Patients with *GBA* mutation did not have causative *PARK2*, *PINK1*, and common *LRRK2* mutations.

p.I(-20)V is an amino acid change in the signal peptide region and was considered to be a single nucleotide polymorphism. The frequency of p.I(-20)V in patients with FPD (13 of 144, 9.0%) was not significantly different from the control subjects (10 of 100 = 10.0%, $p = 0.83$), and its genotype distribution was in Hardy-Weinberg equilibrium in both populations. Although p.K466K mutation was not detected in any control subjects, this synonymous mutation was also excluded for later clinical analyses because it is in a less important region of the final protein.

Two mutations, p.G64V and p.W393X (Fig. 1), were novel, and p.I489V was previously reported in SPD patients (Mitsui et al., 2009). The p.G64V mutation was caused by the substitution of the first amino acid of exon 4, and it seems to be segregated with PD (Figs. 1 and 2). In the family with p.W393X, no affected family member was confirmed for the mutation because of absent genomic DNA. The sequences around the region of mutation were interspecifically conserved in both mutations (Fig. 1).

The recombinant allele Rec*Nci*I was found in 1 patient and 1 control. p.L444P is more common, and p.R120W is less common in Japanese patients with GD, although p.R120W was frequently seen in Japanese FPD patients in the present study (9 of 144 = 6.3%, Table 3). However, p.L444P was the most frequent mutation seen in FPD patients (12 of 144 = 8.3%, Table 3).

In total, we found 31 FPD patients with heterozygous mutations that were reported in GD (p.R120W, p.D409H, p.L444P, c.1447-1466delTGins, and RecNciI) or unreported in GD (p.G64V,

Table 2
Comparison of clinical symptoms between *GBA*-positive and *GBA*-negative patients

Symptom	*GBA* mut (+)	*GBA* mut (−)	p value[a]
N	34	113	
Age at onset (mean ± SD)	49.1 ± 11.7	51.3 ± 14.5	
Resting tremor (%)	18 (52.9)	77 (68.1)	0.151
Bradykinesia (%)	27 (79.4)	99 (87.6)	0.265
Rigidity (%)	29 (85.3)	99 (87.6)	0.772
Gait disturbance (%)	28 (82.4)	95 (84.1)	0.795
Postural instability (%)	20 (58.8)	72 (63.7)	0.687
Wearing off (%)	20 (58.8)	49 (43.4)	0.112
Asymmetry at onset (%)	25 (73.5)	75 (66.4)	0.531
Orthostatic hypotension (%)	5 (14.7)	21 (18.6)	0.798
Incontinence (%)	7 (20.6)	11 (9.7)	0.131
Urinary urgency (%)	10 (29.4)	20 (17.7)	0.150
L-dopa-induced dyskinesia (%)	10 (29.4)	37 (32.7)	0.834
Sleep benefit (%)	3 (8.8)	21 (18.6)	0.288
Dystonia at onset (%)	4 (11.8)	11 (9.7)	0.750
Hyperreflexia (%)	5 (14.7)	17 (15.0)	1.000
Hallucination (%)	14 (41.2)	20 (17.7)	0.009[c]
Delusion (%)	8 (23.5)	6 (5.3)	0.004[c]
Other psychosis (%)	12 (35.3)	11 (9.7)	0.0009[d]
Dementia (%)	12 (35.3)	18 (15.9)	0.027[b]
Gaze palsy (%)	3 (8.8)	2 (1.8)	0.081

[a] Fisher's exact test.
[b] $p < 0.05$.
[c] $p < 0.01$.
[d] $p < 0.001$.

Table 3
Frequency of each *GBA* mutation found in this study

Mutations	FPD (n = 144)	AD (n = 85)	AR (n = 59)	Control (n = 100)	*p* Value[a] (FPD vs. control)	OR (95% CI) (FPD vs. Control)
Reported in GD						
p.R120W (%)	9 (6.3)	9 (10.6)	0 (0)	0 (0)	0.01	NA
p.D409H (%)	4 (2.8)	4 (4.7)	0 (0)	0 (0)	0.14	NA
p.L444P (%)	12 (8.3)	7 (8.2)	5 (8.5)	0 (0)	0.002	NA
indel (%)	1 (0.7)	1 (1.2)	0 (0)	0 (0)	NA	NA
RecNcil (%)	1 (0.7)	1 (1.2)	0 (0)	1 (1)	NA	NA
Unreported in GD						
p.G64V (%)	1 (0.7)	0 (0)	1 (1.7)	0 (0)	NA	NA
p.W393X (%)	1 (0.7)	0 (0)	1 (1.7)	0 (0)	NA	NA
p.I489V (%)	2 (1.4)	1 (1.2)	1 (1.7)	0 (0)	0.51	NA
Total (%)	31 (21.5)	23 (27.1)	8 (13.6)	1 (1)	<0.0001	27.2 (3.6–202.7)

Key: AD, autosomal dominant; AR, autosomal recessive; CI, confidence interval; FPD, familial PD; GD, Gaucher disease; indel, c.1447-1466delTGins; NA, not applicable; OR, odds ratio.
[a] Fisher's exact test. Italics denote novel mutations found in this study.

p.W393X, and p.I489V; Table 3). Interestingly, the frequency of *GBA* mutations among FPD patients was significantly higher than in the controls (31 of 144 = 21.5% vs. 1 of 100 = 1.0%, $p < 0.0001$, odds ratio = 27.2, 95% confidence interval = 3.6–202.7; Table 3). This cohort included 23 ADPD and 8 ARPD of a total of 31 FPD patients. When individual mutations were analyzed, the frequency of the p.R120W and p.*L444P* carriers was significantly higher in index PD patients than in the control subjects ($p = 0.01$ and $p = 0.002$, respectively).

3.2. Mode of inheritance

We compared the differences between groups with AD and AR modes of inheritance and found that the frequency of mutations reported in GD was significantly higher in the AD group than in the AR group (22 of 85 = 25.9% vs. 5 of 59 = 8.5%, $p = 0.009$). Four known mutations reported in GD (p.R120W, p.D409H, c.1447-1466delTGins, and Rec*Ncil*) were all found in the AD group. In 1 AR family (p.L444P) with 2 brothers affected with PD/dementia with Lewy bodies (DLB), the parents had been recorded as asymptomatic, but they died at relatively young ages during the war. Thus, the possibility that this family also should be included in AD family with cosegregation remains (family 28; Fig. 2).

In 2 families with p.L444P and 1 family with p.G64V, both affected siblings had the same mutations, suggesting cosegregation (families 25, 28, and 31; Fig. 2). The present study indicates the incomplete penetrance of p.R120W (families 7 and 9; Fig. 2), which is consistent with previous reports suggesting cosegregation (Mitsui et al., 2009). p.I489V was not considered to show cosegregation (family 35; Fig. 2).

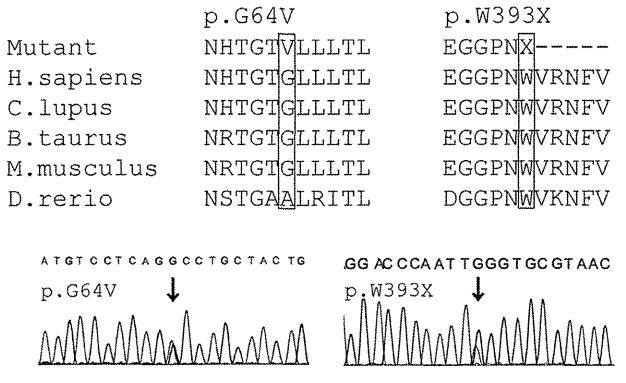

Fig. 1. Novel *GBA* mutations. Genomic sequence chromatogram and comparison of interspecific amino acids around the mutated site.

3.3. Clinical symptoms

In this study, we performed a comparative analysis between 2 groups: *GBA* mutation–positive (n = 34) and *GBA* mutation–-negative patients (n = 113). Clinical and demographic data are listed in Table 2 and Supplementary Table 1. The mean age at onset (AAO) was not significantly different ($p = 0.437$). Statistical analysis of 19 symptoms in PD revealed significant differences in four indexes of hallucination, delirium, dementia, and other psychosis (Table 2). Notably, psychiatric symptoms and/or cognitive decline were more common in *GBA* mutation–positive patients (see Supplementary Table 2). Nine patients with *GBA* mutations underwent cardiac ^{123}I-metaiodobenzylguanidine (MIBG) scintigraphy (see Supplementary Table 3), and all patients showed marked reduction of myocardial MIBG uptake.

4. Discussion

Recently, the largest multicenter analysis of *GBA* mutations has proved an association between *GBA* mutations and PD (Sidransky et al., 2009). To disclose the role of *GBA* in FPD, we performed a *GBA* mutational analysis for in 147 FPD patients from 144 families. The frequency of *GBA* mutations was 21.5% and 25.9% in FPD and ADPD, respectively, which are higher values than reported previously, even compared with SPD patients (Lesage et al., 2011; Mitsui et al., 2009; Sidransky et al., 2009). Therefore, our data suggest that *GBA* mutations play an important role in not only SPD but also FPD, and especially in ADPD. This finding implies that *GBA* could play a major role in FPD and ADPD.

Rare *GBA* mutations have been reported to be a strong risk factor of PD, with a robust odds ratio of 28.0 (Mitsui et al., 2009). Thus, an analysis for *GBA* mutations in FPD was essential to clarify the role of each *GBA* mutation in PD patients. Indeed, p.L444P and p.G64V cosegregated with PD in some families. However, compared with a previous report (Mitsui et al., 2009). p.R120W did not cosegregate in this study. Regarding an association with PD, some mutations remained controversial because of the small number of patients with each mutation and restricted genetic testing in the families. Considering allele frequency, it might be reasonable that *GBA* mutations are incompletely inherited with PD. The carrier frequency of *GBA* mutations was extremely low among the normal Japanese population in this study and in a previous report (Mitsui et al., 2009), whereas many controls among the Jewish population have p.N370S, which is associated with type I GD (Aharon-Peretz et al., 2004), and many controls among the UK population have p.E326K, which is a risk factor for PD (Duran et al., 2013). These racial differences might be derived from the differences of effects of each mutation and other genetic risk factors, which have different

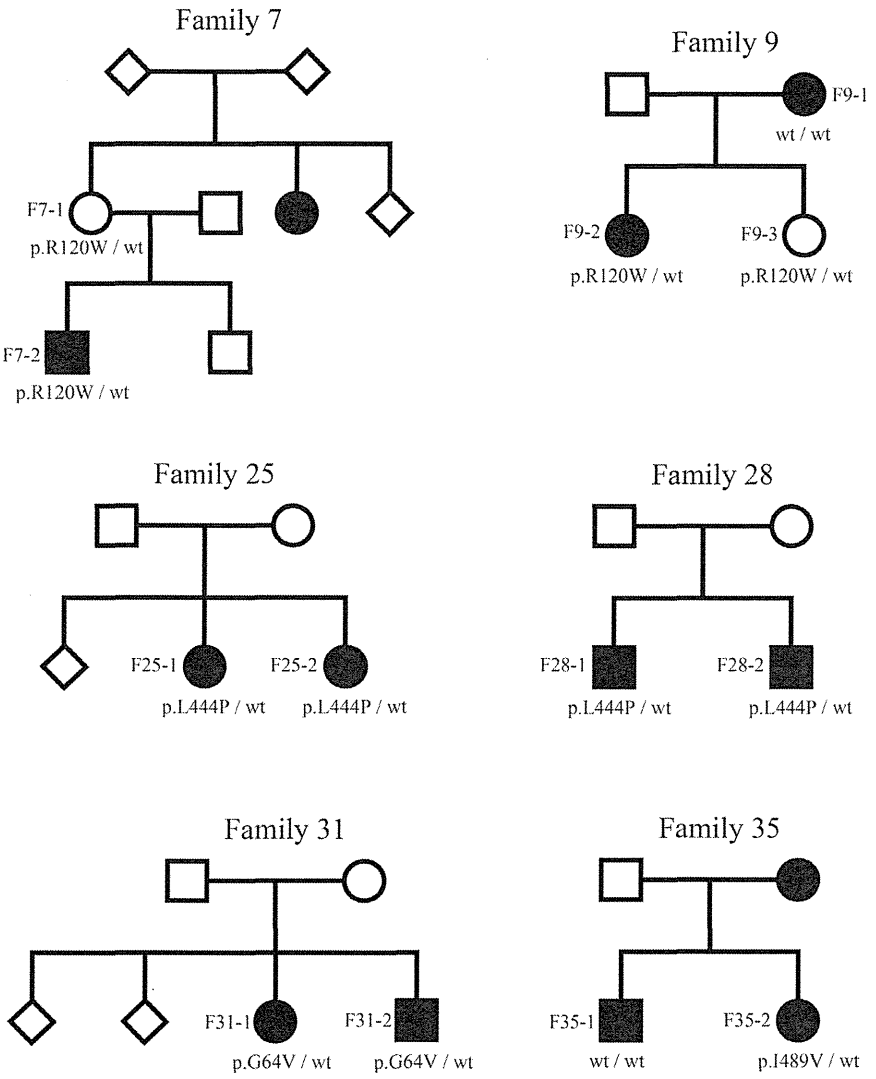

Fig. 2. Cosegregation study of *GBA*-positive families. Pedigrees of families with *GBA* mutations are shown. Affected Parkinson's disease patients are represented with a black symbol. The number of each family member represents his or her patient ID in Supplementary Table 1.

distributions due to founder effects (Lesage et al., 2011; Nishioka et al., 2010; Sidransky et al., 2009). Although racial or regional differences exist for each *GBA* mutation, our data emphasize that *GBA* mutations are more strongly associated with FPD rather than SPD.

A recent study reported a relatively high estimated penetrance ratio in *GBA* carriers, depending on age (7.6%, 13.7%, 21.4%, and 29.7% at 50, 60, 70, and 80 years, respectively). This result should lead to the consideration of *GBA* as a dominant causal gene with reduced penetrance (Anheim et al., 2012). Supporting this consideration, we detected heterozygous *GBA* mutations most frequently in ADPD patients. On the basis of our findings, we conclude that *GBA* is a strong and common risk factor but not a definite causal gene for ADPD and FPD.

In hereditary forms of PD, the frequency of heterozygous *GBA* mutations in ADPD (25.9%) was higher than that observed for ARPD (8.5%). Even allowing for classification bias by definition of ADPD and ARPD, the data imply that *GBA* mutations are strongly associated with ADPD, suggesting that heterozygous *GBA* mutations have a role in familial aggregation, especially in ADPD. In addition, heterozygous mutations have been identified among ARPD patients, suggesting the incomplete penetrance of forms even through the AR mode of inheritance.

Our PD patients with *GBA* mutations frequently developed psychiatric symptoms and/or cognitive decline. Our data support previous results in which PD patients with *GBA* mutations manifest exacerbated psychiatric symptoms and/or cognitive decline compared to those without *GBA* mutations (Alcalay et al., 2012; Sidransky et al., 2009; Winder-Rhodes et al., 2013). Some previous studies have reported the association of *GBA* mutations and DLB (Clark et al., 2009; Nalls et al., 2013; Tsuang et al., 2012). Our data further suggest that *GBA* heterozygous mutation carriers can develop clinical symptoms of PD and DLB. Accordingly, we found decreased cardiac MIBG uptake associated with *GBA* mutations. The heart-to-mediastinum ratio correlated with PD/DLB clinical severity; a decreasing ratio corresponded to an ascending Hoehn and Yahr stage (Nagayama et al., 2005). Thus, MIBG scintigraphy could be a useful biomarker for PD/Lewy body disease in patients with *GBA* mutations.

Lewy body diseases are alpha-synucleinopathies characterized by abnormal accumulation of alpha-synuclein in neuronal cytoplasm. Recently, biochemical analysis using cell and animal models demonstrated that some *GBA* mutations lead to increased alpha-

synuclein concentration (Cullen et al., 2011). *GBA* mutation may promote alpha-synuclein accumulation and Lewy body development via the aberrant lysosomal function, resulting in severe parkinsonism and cognitive decline associated with DLB (Mazzulli et al., 2011; Tsuang et al., 2012; Yap et al., 2013).

Collectively, our findings have major implications for the genetic and pathogenic mechanisms of *GBA*. GD is an autosomal recessive disorder caused by mutations in both *GBA* alleles, which leads to a loss of function or reduced enzyme activity. In contrast to GD, our FPD and ADPD patients carried 1 mutant allele and 1 wild-type *GBA* allele. Therefore, the pathogenic mechanism may be due to haploinsufficiency, dominant-negative effect, or toxic gain of function rather than a loss of function.

In conclusion, heterozygous *GBA* mutations play a greater role in FPD, especially in ADPD, and are likely to facilitate the development of PD and Lewy body diseases via different genetic and pathogenic mechanisms. Our findings suggest that further functional analyses for *GBA* should elucidate the pathogenesis of PD and Lewy body diseases.

Disclosure statement

The authors have no actual or potential conflicts of interest.

Acknowledgements

This work was supported by the Strategic Research Foundation Grant-in-Aid Project for Private Universities, Grant-in-Aid for Young Scientists (to MF, 22790829 and to YL, 23791003), Grant-in-Aid for Scientific Research (to NH, 80218510 and to HT, 21591098), Grants-in-Aid from the Research Committee of CNS Degenerative Diseases, the Ministry of Health, Labour and Welfare of Japan (to NH, and to HT: 22140901) Grant-in-Aid for Scientific Research on Innovative Areas (to NH, 23111003 and to MF, 23129506) from the Japanese Ministry of Education, Culture, Sports, Science, and Technology, Grants from Health and Labor Sciences Research, Grants from Japanese Ministry of Health, Labor and Welfare (to NH, 20261501, 22140501, 22140901, and 23111003), and JST, CREST. The authors thank the study participants and Dr Jun Mitsui for technical advice. We are grateful to Dr Fusako Yokochi, Dr Daita Kaneda, Dr Kenichi Kashihara, Dr Masatoshi Omoto, and Dr Kyugo Hirabayashi for providing the patient clinical information. The authors also thank Ms Yoko Imamichi for technical assistance.

Appendix A. Supplementary data

Supplementary data associated with this article can be found, in the online version, at http://dx.doi.org/10.1016/j.neurobiolaging.2013.09.019.

References

Aharon-Peretz, J., Rosenbaum, H., Gershoni-Baruch, R., 2004. Mutations in the glucocerebrosidase gene and Parkinson's disease in Ashkenazi Jews. N. Engl. J. Med. 351, 1972–1977.

Alcalay, R.N., Caccappolo, E., Mejia-Santana, H., Tang, M.X., Rosado, L., Orbe Reilly, M., Ruiz, D., Ross, B., Verbitsky, M., Kisselev, S., Louis, E., Comella, C., Colcher, A., Jennings, D., Nance, M., Bressman, S., Scott, W.K., Tanner, C., Mickel, S., Andrews, H., Waters, C., Fahn, S., Cote, L., Frucht, S., Ford, B., Rezak, M., Novak, K., Friedman, J.H., Pfeiffer, R., Marsh, L., Hiner, B., Siderowf, A., Payami, H., Molho, E., Factor, S., Ottman, R., Clark, L.N., Marder, K., 2012. Cognitive performance of GBA mutation carriers with early-onset PD: the CORE-PD study. Neurology 78, 1434–1440.

Anheim, M., Elbaz, A., Lesage, S., Durr, A., Condroyer, C., Viallet, F., Pollak, P., Bonaiti, B., Bonaiti-Pellie, C., Brice, A., 2012. Penetrance of Parkinson disease in glucocerebrosidase gene mutation carriers. Neurology 7, 417–420.

Clark, L.N., Kartsaklis, L.A., Wolf Gilbert, R., Dorado, B., Ross, B.M., Kisselev, S., Verbitsky, M., Mejia-Santana, H., Cote, L.J., Andrews, H., Vonsattel, J.P., Fahn, S., Mayeux, R., Honig, L.S., Marder, K., 2009. Association of glucocerebrosidase mutations with dementia with lewy bodies. Arch. Neurol. 66, 578–583.

Cullen, V., Sardi, S.P., Ng, J., Xu, Y.H., Sun, Y., Tomlinson, J.J., Kolodziej, P., Kahn, I., Saftig, P., Woulfe, J., Rochet, J.C., Glicksman, M.A., Cheng, S.H., Grabowski, G.A., Shihabuddin, L.S., Schlossmacher, M.G., 2011. Acid beta-glucosidase mutants linked to Gaucher disease, Parkinson disease, and Lewy body dementia alter alpha-synuclein processing. Ann. Neurol. 69, 940–953.

Duran, R., Mencacci, N.E., Angeli, A.V., Shoai, M., Deas, E., Houlden, H., Mehta, A., Hughes, D., Cox, T.M., Deegan, P., Schapira, A.H., Lees, A.J., Limousin, P., Jarman, P.R., Bhatia, K.P., Wood, N.W., Hardy, J., Foltynie, T., 2013. The glucocerebrosidase E326K variant predisposes to Parkinson's disease, but does not cause Gaucher's disease. Mov. Disord. 28, 232–236.

Folstein, M.F., Folstein, S.E., McHugh, P.R., 1975. "Mini-Mental State". A practical method for grading the cognitive state of patients for the clinician. J. Psychiatr. Res. 12, 189–198.

Hamza, T.H., Zabetian, C.P., Tenesa, A., Laederach, A., Montimurro, J., Yearout, D., Kay, D.M., Doheny, K.F., Paschall, J., Pugh, E., Kusel, V.I., Collura, R., Roberts, J., Griffith, A., Samii, A., Scott, W.K., Nutt, J., Factor, S.A., Payami, H., 2010. Common genetic variation in the HLA region is associated with late-onset sporadic Parkinson's disease. Nat. Genet. 4, 781–785.

Hatano, T., Kubo, S., Sato, S., Hattori, N., 2009. Pathogenesis of familial Parkinson's disease: new insights based on monogenic forms of Parkinson's disease. J. Neurochem. 111, 1075–1093.

Hruska, K.S., LaMarca, M.E., Scott, C.R., Sidransky, E., 2008. Gaucher disease: mutation and polymorphism spectrum in the glucocerebrosidase gene (GBA). Hum. Mutat. 29, 567–583.

Hughes, A.J., Daniel, S.E., Kilford, L., Lees, A.J., 1992. Accuracy of clinical diagnosis of idiopathic Parkinson's disease: a clinico-pathological study of 100 cases. J. Neurol. Neurosurg. Psychiatry 55, 181–184.

Lesage, S., Anheim, M., Condroyer, C., Pollak, P., Durif, F., Dupuits, C., Viallet, F., Lohmann, E., Corvol, J.C., Honore, A., Rivaud, S., Vidailhet, M., Durr, A., Brice, A., 2011. Large-scale screening of the Gaucher's disease-related glucocerebrosidase gene in Europeans with Parkinson's disease. Hum. Mol. Genet. 20, 202–210.

Mazzulli, J.R., Xu, Y.H., Sun, Y., Knight, A.L., McLean, P.J., Caldwell, G.A., Sidransky, E., Grabowski, G.A., Krainc, D., 2011. Gaucher disease glucocerebrosidase and alpha-synuclein form a bidirectional pathogenic loop in synucleinopathies. Cell 146, 37–52.

Mitsui, J., Mizuta, I., Toyoda, A., Ashida, R., Takahashi, Y., Goto, J., Fukuda, Y., Date, H., Iwata, A., Yamamoto, M., Hattori, N., Murata, M., Toda, T., Tsuji, S., 2009. Mutations for Gaucher disease confer high susceptibility to Parkinson disease. Arch. Neurol. 66, 571–576.

Nagayama, H., Hamamoto, M., Ueda, M., Nagashima, J., Katayama, Y., 2005. Reliability of MIBG myocardial scintigraphy in the diagnosis of Parkinson's disease. J. Neurol. Neurosurg. Psychiatry 76, 249–251.

Nalls, M.A., Duran, R., Lopez, G., Kurzawa-Akanbi, M., McKeith, I.G., Chinnery, P.F., Morris, C.M., Theuns, J., Crosiers, D., Cras, P., Engelborghs, S., De Deyn, P.P., Van Broeckhoven, C., Mann, D.M., Snowden, J., Pickering-Brown, S., Halliwell, N., Davidson, Y., Gibbons, L., Harris, J., Sheerin, U.M., Bras, J., Hardy, J., Clark, L., Marder, K., Honig, L.S., Berg, D., Maetzler, W., Brockmann, K., Gasser, T., Novellino, F., Quattrone, A., Annesi, G., De Marco, E.V., Rogaeva, E., Masellis, M., Black, S.E., Bilbao, J.M., Foroud, T., Ghetti, B., Nichols, W.C., Pankratz, N., Halliday, G., Lesage, S., Klebe, S., Durr, A., Duyckaerts, C., Brice, A., Giasson, B.I., Trojanowski, J.Q., Hurtig, H.I., Tayebi, N., Landazabal, C., Knight, M.A., Keller, M., Singleton, A.B., Wolfsberg, T.G., Sidransky, E., 2013. A multicenter study of glucocerebrosidase mutations in dementia with Lewy bodies. JAMA Neurol. 70, 727–735.

Nishioka, K., Vilarino-Guell, C., Cobb, S.A., Kachergus, J.M., Ross, O.A., Wider, C., Gibson, R.A., Hentati, F., Farrer, M.J., 2010. Glucocerebrosidase mutations are not a common risk factor for Parkinson disease in North Africa. Neurosci. Lett. 477, 57–60.

Satake, W., Nakabayashi, Y., Mizuta, I., Hirota, Y., Ito, C., Kubo, M., Kawaguchi, T., Tsunoda, T., Watanabe, M., Takeda, A., Tomiyama, H., Nakashima, K., Hasegawa, K., Obata, F., Yoshikawa, T., Kawakami, H., Sakoda, S., Yamamoto, M., Hattori, N., Murata, M., Nakamura, Y., Toda, T., 2009. Genome-wide association study identifies common variants at four loci as genetic risk factors for Parkinson's disease. Nat. Genet. 41, 1303–1307.

Sidransky, E., Nalls, M.A., Aasly, J.O., Aharon-Peretz, J., Annesi, G., Barbosa, E.R., Bar-Shira, A., Berg, D., Bras, J., Brice, A., Chen, C.M., Clark, L.N., Condroyer, C., De Marco, E.V., Durr, A., Eblan, M.J., Fahn, S., Farrer, M.J., Fung, H.C., Gan-Or, Z., Gasser, T., Gershoni-Baruch, R., Giladi, N., Griffith, A., Gurevich, T., Januario, C., Kropp, P., Lang, A.E., Lee-Chen, G.J., Lesage, S., Marder, K., Mata, I.F., Mirelman, A., Mitsui, J., Mizuta, I., Nicoletti, G., Oliveira, C., Ottman, R., Orr-Urtreger, A., Pereira, L.V., Quattrone, A., Rogaeva, E., Rolfs, A., Rosenbaum, H., Rozenberg, R., Samii, A., Samaddar, T., Schulte, C., Sharma, M., Singleton, A., Spitz, M., Tan, E.K., Tayebi, N., Toda, T., Troiano, A.R., Tsuji, S., Wittstock, M., Wolfsberg, T.G., Wu, Y.R., Zabetian, C.P., Zhao, Y., Ziegler, S.G., 2009. Multicenter analysis of glucocerebrosidase mutations in Parkinson's disease. N. Engl. J. Med. 361, 1651–1661.

Simon-Sanchez, J., Schulte, C., Bras, J.M., Sharma, M., Gibbs, J.R., Berg, D., Paisan-Ruiz, C., Lichtner, P., Scholz, S.W., Hernandez, D.G., Kruger, R., Federoff, M., Klein, C., Goate, A., Perlmutter, J., Bonin, M., Nalls, M.A., Illig, T., Gieger, C., Houlden, H., Steffens, M., Okun, M.S., Racette, B.A., Cookson, M.R., Foote, K.D., Fernandez, H.H., Traynor, B.J., Schreiber, S., Arepalli, S., Zonozi, R., Gwinn, K., van

der Brug, M., Lopez, G., Chanock, S.J., Schatzkin, A., Park, Y., Hollenbeck, A., Gao, J., Huang, X., Wood, N.W., Lorenz, D., Deuschl, G., Chen, H., Riess, O., Hardy, J.A., Singleton, A.B., Gasser, T., 2009. Genome-wide association study reveals genetic risk underlying Parkinson's disease. Nat. Genet. 41, 1308–1312.

Tsuang, D., Leverenz, J.B., Lopez, O.L., Hamilton, R.L., Bennett, D.A., Schneider, J.A., Buchman, A.S., Larson, E.B., Crane, P.K., Kaye, J.A., Kramer, P., Woltjer, R., Kukull, W., Nelson, P.T., Jicha, G.A., Neltner, J.H., Galasko, D., Masliah, E., Trojanowski, J.Q., Schellenberg, G.D., Yearout, D., Huston, H., Fritts-Penniman, A., Mata, I.F., Wan, J.Y., Edwards, K.L., Montine, T.J., Zabetian, C.P., 2012. GBA mutations increase risk for Lewy body disease with and without Alzheimer disease pathology. Neurology 79, 1944–1950.

Tsuji, S., Choudary, P.V., Martin, B.M., Stubblefield, B.K., Mayor, J.A., Barranger, J.A., Ginns, E.I., 1987. A mutation in the human glucocerebrosidase gene in neuronopathic Gaucher's disease. N. Engl. J. Med. 316, 570–575.

Weintraub, D., Burn, D.J., 2011. Parkinson's disease: the quintessential neuropsychiatric disorder. Mov. Disord. 26, 1022–1031.

Winder-Rhodes, S.E., Evans, J.R., Ban, M., Mason, S.L., Williams-Gray, C.H., Foltynie, T., Duran, R., Mencacci, N.E., Sawcer, S.J., Barker, R.A., 2013. Glucocerebrosidase mutations influence the natural history of Parkinson's disease in a community-based incident cohort. Brain 136, 392–399.

Yap, T.L., Velayati, A., Sidransky, E., Lee, J.C., 2013. Membrane-bound alpha-synuclein interacts with glucocerebrosidase and inhibits enzyme activity. Mol. Genet. Metab. 108, 56–64.

RESEARCH COMMUNICATION

Tricornered/NDR kinase signaling mediates PINK1-directed mitochondrial quality control and tissue maintenance

Zhihao Wu,[1] Tomoyo Sawada,[2,3] Kahori Shiba,[4] Song Liu,[1] Tomoko Kanao,[5] Ryosuke Takahashi,[2,3] Nobutaka Hattori,[4,5,6] Yuzuru Imai,[6,7] and Bingwei Lu[1,7]

[1]Department of Pathology, Stanford University School of Medicine, Stanford, California 94305, USA; [2]Department of Neurology, Graduate School of Medicine, Kyoto University, Kyoto 606-8507, Japan; [3]CREST (Core Research for Evolutionary Science and Technology), Japan Science and Technology Agency, Saitama 332-0012, Japan; [4]Department of Neurology, Juntendo University Graduate School of Medicine, Tokyo 113-8421, Japan; [5]Research Institute for Diseases of Old Age, Juntendo University Graduate School of Medicine, Tokyo 113-8421, Japan; [6]Department of Neuroscience for Neurodegenerative Disorders, Juntendo University Graduate School of Medicine, Tokyo 113-8421, Japan

Eukaryotes employ elaborate mitochondrial quality control (MQC) to maintain the function of the power-generating organelle. Parkinson's disease-associated PINK1 and Parkin actively participate in MQC. However, the signaling events involved are largely unknown. Here we show that mechanistic target of rapamycin 2 (mTORC2) and Tricornered (Trc) kinases act downstream from PINK1 to regulate MQC. Trc is phosphorylated in mTORC2-dependent and mTORC2-independent manners and is specifically localized to mitochondria in response to PINK1, which regulates mTORC2 through mitochondrial complex-I activity. Genetically, mTORC2 and Trc act upstream of Parkin. Thus, multiplex kinase signaling is acting between PINK1 and Parkin to regulate MQC, a process highly conserved in mammals.

Supplemental material is available for this article.

Received August 13, 2012; revised version accepted December 4, 2012.

To sustain energy supply and overall cellular health, elaborate quality control systems are deployed to maintain mitochondrial integrity and functionality (Narendra and Youle 2011; Rugarli and Langer 2012). Mitochondrial quality control (MQC) is particularly important for the maintenance of neural and muscular tissues. PINK1 (Valente et al. 2004) and Parkin (Kitada et al. 1998), two proteins associated with familial Parkinson's disease (PD), have been identified as central players in a cellular pathway that directs MQC, a dynamic and multifaceted network encompassing mitochondrial complex-I (CI) function (Liu et al. 2011; Vilain et al. 2012), fission/fusion dynamics (Yang et al. 2008), transport (Wang et al. 2011; Liu et al. 2012), and mitophagy (Liu and Lu 2010; Narendra et al. 2010). Genetic epistasis studies, first in *Drosophila* (Clark et al. 2006; Park et al. 2006; Yang et al. 2006) and later in mammalian cells (Exner et al. 2007), positioned PINK1 upstream of Parkin in MQC. Studies in mammalian cells have further shown that PINK1 becomes stabilized on the outer membrane of depolarized mitochondria, where it recruits Parkin from the cytosol to promote mitophagy (Narendra et al. 2010). However, the mechanisms of PINK1 and Parkin action and the signaling events involved in the MQC process are poorly understood, with various discordant models having been proposed (Narendra and Youle 2011).

We continued using the powerful tools available in *Drosophila* to dissect the genetic program underlying PINK1/Parkin-directed MQC. Here we identify mechanistic target of rapamycin 2 (mTORC2) and tricornered (Trc) kinase signaling as intermediate steps between PINK1 and Parkin in the MQC process in *Drosophila* and further verify the findings in mammalian cells. Our results reveal a previously unanticipated complexity of signaling events involved in PINK1/Parkin-directed MQC and tissue maintenance and shed new light on how mTORC2 and Trc, two important kinases critically involved in cellular morphogenesis, development, growth, and disease, are regulated in an in vivo setting.

Results and Discussion

To elucidate the signaling events acting downstream from PINK1, we performed genetic screens as described before (Liu and Lu 2010; Liu et al. 2012) to identify genes that can modify PINK1 loss-of-function (LOF)-induced wing posture and flight ability defects. This led to the identification of mTORC2 components as strong modifiers of PINK1. While overexpression of the mTORC2 components Rictor and Sin1 (Hietakangas and Cohen 2007), either individually or in combination, had no obvious effects on their own (Supplemental Fig. S1), they effectively suppressed *dPINK1* LOF phenotypes with respect to the integrity and function of flight muscle, as measured by thoracic ATP level and wing posture (Fig. 1A,B;Supplemental Fig. S1D) and the loss of dopaminergic neurons (DNs) in the PPL1 cluster (Fig. 1E). Conversely, *rictor* or *sin1* mutations significantly enhanced *dPINK1* LOF phenotypes (Fig. 1A–E; Supplemental Fig. S1D), although the *rictor* or *sin1* mutant alone did not show obvious phenotypes in these assays (Supplemental Fig. S1A–C). The effects of mTORC2 components on tissue integrity correlated well with the effects on mitochondrial morphology, with mTORC2 gain of function (GOF) rescuing the mitochondrial aggregation phenotype caused by *dPINK1* LOF, whereas mTORC2 LOF had opposite effects (Fig. 1C,D).

We next explored the molecular mechanisms underlying the strong genetic interaction between PINK1 and mTORC2. Using phosphorylation of *Drosophila* AKT at S505 as readout of mTORC2 activity (Sarbassov et al.

[*Keywords*: Tricornered; NDR; mTORC2; PINK1; mitochondrial quality control]
[7]**Corresponding authors**
E-mail bingwei@stanford.edu
E-mail yzimai@juntendo.ac.jp
Article is online at http://www.genesdev.org/cgi/doi/10.1101/gad.203406.112.

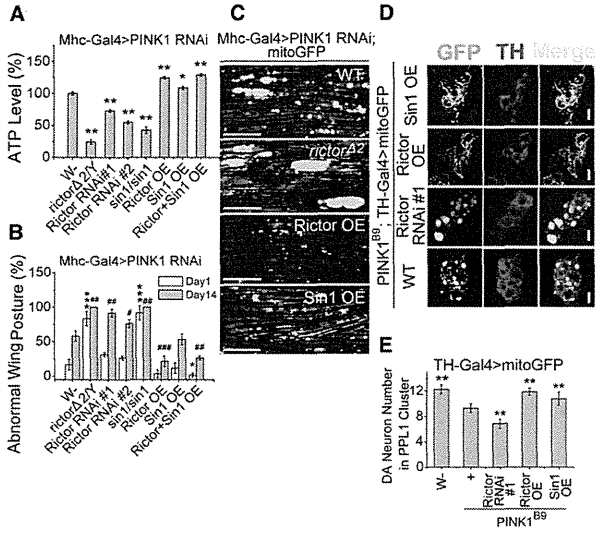

Figure 1. Genetic interaction between PINK1 and mTORC2. (*A*) PINK1 RNAi-induced ATP level drop was rescued by Rictor or Sin1 overexpression (OE) but enhanced by their LOF. (*B*) PINK1 RNAi-induced abnormal wing posture was rescued by Rictor overexpression or Rictor + Sin1 overexpression but enhanced by their LOF. (*C*) PINK1 RNAi-induced mitochondrial aggregation in muscle was strongly rescued by Rictor overexpression and moderately rescued by Sin1 overexpression but was enhanced by *rictor* LOF. Mitochondrial morphology was monitored with a mito-GFP reporter. Bar, 30 μm. (*D*) PINK1 LOF-induced mitochondrial aggregation in DNs was strongly rescued by Rictor overexpression and moderately rescued by Sin1 overexpression but enhanced by *rictor* LOF. Bar, 5 μm. (*E*) PINK1 LOF-induced loss of DNs in the PPL1 cluster was rescued by Rictor overexpression but enhanced by *rictor* LOF. A *rictor* deletion mutant (Δ2) and two independent *rictor* RNAi lines (#1 and #2) were used in LOF studies. (* or #) $P < 0.05$; (** or ##) $P < 0.01$; (*** or ###) $P < 0.005$ in one-way ANOVA tests when data from day 1 or day 14 were compared.

2005), we found that the p-S505-AKT level was significantly reduced in the *dPINK1* LOF condition but increased by PINK1 GOF (Fig. 2A), indicating that PINK1 regulates mTORC2 activity in vivo. To further validate this point, we affinity-purified *Drosophila* mTORC2 from transgenic animals expressing a Flag-tagged Sin1 (Koike-Kumagai et al. 2009). In vitro kinase assays using purified mTORC2 as the kinase and kinase-dead (KD) GST-AKT as the substrate showed that the specific activity of mTORC2 was reduced in the *dPINK1*^{B9}-null mutant but increased in PINK1 GOF background (Fig. 2B). The amounts of dTOR copurifying with Flag-Sin1 were comparable among the various genotypes (Fig. 2B), suggesting that PINK1 primarily regulates mTORC2 kinase activity instead of its assembly. Consistent with impaired mTORC2 signaling contributing to PINK1 pathogenesis, phosphatidylinositol 3,4,5-trisphosphate (PIP_3) treatment, which could directly activate mTORC2 in mammalian cells (Gan et al. 2011), partially restored mTORC2 activity (Fig. 2C,D) and rescued *dPINK1* mutant phenotypes in terms of lifespan, wing posture, and mitochondrial morphology (Fig. 2E–G).

Despite the importance of mTORC2 in physiology and disease, little is known about how it is regulated by upstream signals (Zoncu et al. 2011). We further investigated how PINK1 regulates mTORC2 activity. Given that PINK1 is a mitochondrial resident protein intimately linked to CI function and that CI dysfunction could phenocopy *dPINK1* LOF effects (Supplemental Fig. S2A–C), we reasoned that the functional status of CI might affect mTORC2 activity. To test this hypothesis, we first examined p-S505-AKT levels in wild-type animals treated with the CI inhibitor rotenone (Fig. 2H) or with CI subunits knocked down by RNAi (Fig. 2I). These manipulations led to decreased p-S505-AKT levels. Consistently, mTORC2 purified from CI-impaired animals exhibited reduced kinase activity in vitro (Supplemental Fig. S2D). Importantly, in *dPINK1* mutants whose CI activity was supplemented by yeast NADH ubiquinone oxidoreductase (yNDI1), the mutant phenotypes were effectively rescued (Supplemental Fig. S2E–G), consistent with a recent study (Vilain et al. 2012), and p-S505-AKT level was restored to normal (Fig. 2I). Further supporting a functional link between CI and mTORC2 activation, mTORC2 LOF animals were particularly sensitive to rotenone treatment compared with other stress treatments (Supplemental Fig. S3A–F), and LOF of mTORC2 and CI synergistically disrupted muscle function (Supplemental Fig. S3G). These results demonstrate that the functional state of CI maintained by PINK1 is a critical determinant of mTORC2 activity. Supporting this notion, PINK1 was found to associate with components of CI (Supplemental Fig. S2H).

Next, we sought to determine the signaling events downstream from mTORC2 that mediate PINK1-directed MQC and tissue maintenance. Surprisingly, even though AKT is considered a key downstream target of mTORC2 (Wullschleger et al. 2006; Russell et al. 2011; Zoncu et al. 2011) and AKT function is compromised in the *dPINK1* mutant, as shown by a reduced p-S505-AKT level, overexpression of wild-type or phospho-mutant forms of AKT had no obvious effect on *dPINK1* LOF phenotypes in terms of mitochondrial morphology and tissue maintenance (Supplemental Fig. S4A–C). Knocking down AKT by RNAi also had no obvious effect (Supplemental Fig. S4A–C). Thus, the best-studied mTORC2 target, AKT, is unlikely to be a key mediator of mTORC2 function in PINK1-controlled MQC and tissue maintenance.

Trc kinase was recently identified as a downstream effector of mTORC2 in regulating the dendritic tiling of *Drosophila* sensory neurons (Koike-Kumagai et al. 2009). Trc was originally isolated in a screen for genes affecting wing hair morphogenesis (Geng et al. 2000) and was later found to be important for dendritic patterning (Emoto et al. 2004) in *Drosophila*. Trc is homologous to mammalian nuclear Dbf-2-related (NDR) kinases (Hergovich et al. 2006). Whether Trc/NDR regulates mitochondrial function or neuromuscular tissue maintenance is not known. Interestingly, although overexpression of Trc LOF or GOF transgenes alone had little effect on muscle function (Supplemental Fig. S5A–C), Trc GOF transgenes effectively suppressed *dPINK1* LOF phenotypes in muscle (Fig. 3A,B; Supplemental Fig. S5D) or DN (Fig. 3E) maintenance and mitochondrial morphology (Fig. 3C,D), whereas dominant-negative Trc (Trc-K122A or Trc-K122/T453A) had opposite effects (Fig. 3A–E; Supplemental Fig. S5D). Note that wild-type or constitutively active Trc (Trc-S292E and Trc-T453E) were equally effective in the GOF assays, indicating that overexpressed wild-type Trc became sufficiently activated, as indicated by its high level phosphorylation at S292 (Fig. 3F).

Consistent with Trc acting downstream from mTORC2, the enhancement of *dPINK1* LOF phenotypes by *rictor* mutation was attenuated by wild-type Trc (Trc-WT) or Trc-S292E GOF transgenes (Supplemental Fig. S6A,C),

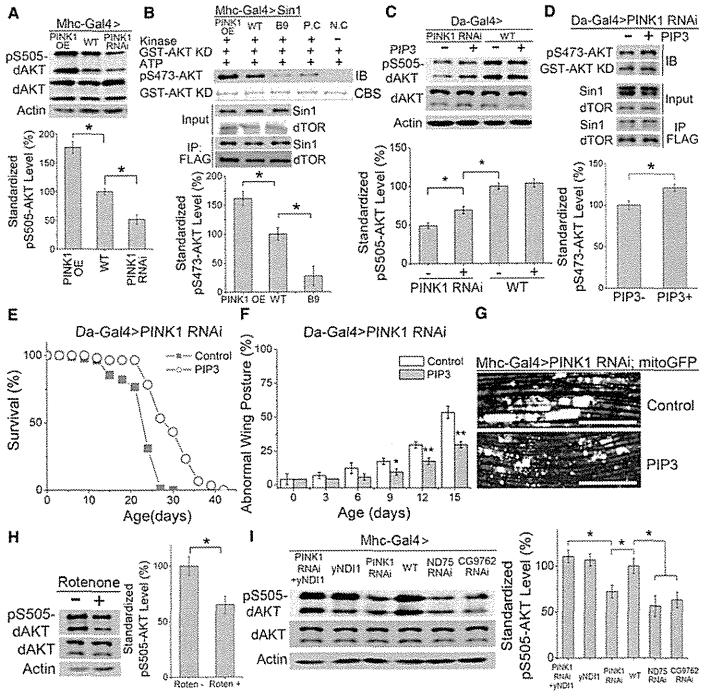

Figure 2. Effects of PINK1 and mitochondrial CI function on TORC2 activity. (*A*) Western blot analysis of *Mhc-Gal4*-driven control (wild type [WT]), PINK1 overexpression, and PINK1-RNAi muscle extracts with the indicated antibodies and data quantification. (*B*, *top*) In vitro phosphorylation of recombinant human GST-AKT-KD by *Drosophila* TORC2 affinity-purified from control, PINK1-overexpressing, and PINK1 LOF animals, all expressing a Sin1-Flag transgene. (*Bottom*) Similar amounts of Sin1 and dTOR were present in the extracts or immunoprecipitated TORC2. After kinase reaction, AKT phosphorylation was detected with anti-pS473-AKT, and total GST-AKT-KD was detected by Coomassie Blue staining (CBS). (P.C.) Positive control with extract added; (N.C.) negative control with no kinase added. Bar graph shows data quantification. (*C–G*) The rescuing effect of PIP3 treatment on in vivo p-S505-AKT level (*C*), in vitro mTORC2 kinase activity (*D*), lifespan (*E*), wing posture (*F*), and muscle mitochondrial morphology (*G*) in PINK1-RNAi animals. Values represent relative protein amounts after normalization with controls. Mitochondrial morphology was monitored with a mito-GFP reporter. In vitro mTORC2 kinase assay was performed as in *B*. Bar graphs show data quantification. Bar, 30 μm. (*H*) Reduction of pS505-AKT level by rotenone treatment of wild-type animals. (*I*) Effect of CI subunit (ND75 and CG9762) RNAi on pS505-AKT level and restoration of the p-S505-AKT level in PINK1-RNAi animals after yNDI1 coexpression. Values represent relative protein amounts after normalization with controls. Bar graphs show data quantification. (*) $P < 0.05$ in one-way ANOVA or Student's *t*-tests.

whereas the rescue of *dPINK1* LOF phenotypes by Rictor overexpression was fully blocked by Trc LOF transgenes (Supplemental Fig. S6B,D). Moreover, Trc RNAi induced mitochondrial aggregation and DN loss in a wild-type background (Supplemental Fig. S7A–C). These results thus establish Trc as a key component of the PINK1 pathway in MQC and tissue maintenance.

We further explored the biochemical mechanism of the signaling events involving PINK1, mTORC2, and Trc. Consistent with Trc acting downstream from PINK1, phosphorylation of Trc at S292 and T453, which correlate with Trc activation (Emoto et al. 2006), were reduced in *dPINK1* mutants but significantly increased in PINK1 GOF flies (Fig. 3F). This was further supported by in vitro assays of kinase activities of Trc purified from PINK1 LOF and GOF flies using phosphorylation of AAK1, a newly identified substrate of mammalian NDR (Ultanir et al. 2012), as readout (Fig. 3G). Interestingly, the effect of PINK1 on T453 site phosphorylation was mTORC2-dependent, whereas its effect on S292 was mTORC2-independent (Fig. 3H), suggesting that PINK1 regulates these two phosphorylation events through distinct mechanisms. We next tested whether activated Trc is localized to mitochondria to exert its effects on MQC. Strikingly, p-T453-Trc and p-S292-Trc were found primarily in the mitochondrial fraction, whereas total Trc was found in both the cytoplasmic and mitochondrial fractions (Supplemental Fig. S8A). Since mTORC2 is also localized to mitochondria (Supplemental Fig. S8B), mitochondria may serve as a novel platform for mTORC2 and Trc signaling.

Parkin plays a critical role in MQC and maintenance of muscle and DNs and acts downstream from PINK1. We found that the LOF effects of Rictor (Fig. 4A,E) or Trc (Fig. 4C,G) in enhancing *dPINK1* mutant phenotypes were completely blocked by Parkin GOF, suggesting that Parkin acts downstream from TORC2 and Trc in the PINK1 pathway. Consistently, Rictor GOF (Fig. 4B,F) or Trc GOF (Fig. 4D,H) failed to rescue the abnormal wing posture and mitochondrial morphology phenotypes of the *parkin* mutant. Next, we tested the genetic interaction between mTORC2/Trc and key executors of MQC known to genetically interact with PINK1, including the mitochondrial fusion protein Marf (Liu and Lu 2010; Ziviani et al. 2010), the autophagy regulator Atg1 (Liu and Lu 2010), and the mitochondrial transport protein Miro (Wang et al. 2011; Liu et al. 2012). Marf RNAi or Atg1 GOF effectively blocked the enhancing effects of mTORC2 LOF (Fig. 4I,J) or Trc LOF (Fig. 4K,L) in the *dPINK1* mutant background. Miro RNAi was also effective, although to a lesser degree (Fig. 4I–L). Together, these genetic epistasis data support critical roles of mTORC2 and Trc in mediating the effect of PINK1 in MQC and tissue maintenance.

In mammalian cells, the PINK1–Parkin pathway also plays central roles in MQC, with Parkin recruited to damaged mitochondria in a PINK1-dependent manner to promote mitophagy (Narendra et al. 2010). We tested whether the mammalian Trc homologs NDR1/2 act in PINK1/Parkin-directed MQC. Knockdown of NDR1 but not NDR2 in HeLa cells led to altered mitochondrial distribution, compromised recruitment of Parkin by PINK1, and delayed clearance of damaged mitochondria (Supplemental Fig. S9A–C). The mitophagy defects induced by NDR1 RNAi were rescued by a siRNA-resistant NDR1 construct (Supplemental Fig. S9B,D). Importantly, we detected reduced phosphorylation of NDR1 at the corresponding T444 site in *PINK1*$^{-/-}$ mouse embryonic fibroblasts (MEFs) expressing a kinase-dead form of PINK1 but not wild-type PINK1 (Supplemental Fig. S10). Due to the hypersensitivity of p-NDR1 to endogenous phosphatase activities as previously reported (Koike-Kumagai et al. 2009), treatment with okadaic acid (OA) was needed to reveal the effect of PINK1 on the p-NDR1 level. These results support that NDR1 acts in the PINK1/Parkin pathway in mammals. In carbonyl cyanide m-chlorophe-

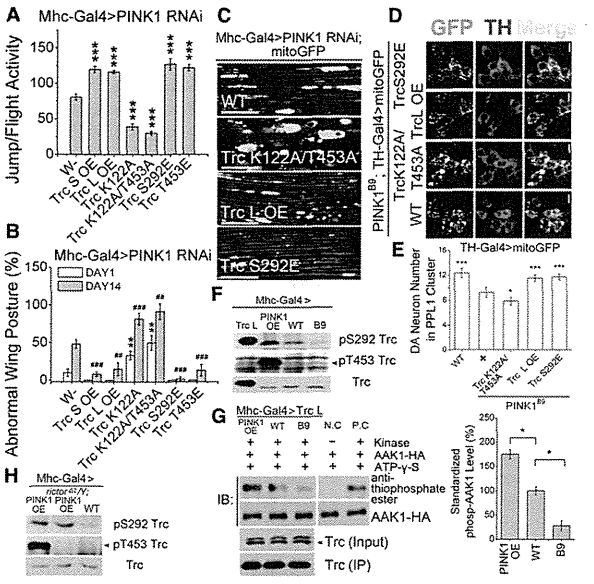

Figure 3. Evidence that Trc acts in the PINK1 pathway. (*A*,*B*) *Mhc-Gal4>PINK1 RNAi*-induced flight ability (*A*) and wing posture (*B*) defects were rescued by the coexpression of the short (S) or long (L) isoforms of wild-type Trc or constitutively active (S292E or T453E) Trc but enhanced by dominant-negative (K122A or K122A/T453A) Trc. (* or #) $P < 0.05$; (** or ##) $P < 0.01$; (*** or ###) $P < 0.005$ in one-way ANOVA tests when data from day 1 (*) or day 14 (#) were compared. (*C*) *Mhc-Gal4>PINK1 RNAi*-induced mitochondrial aggregation in indirect flight muscle was rescued by the coexpression of Trc-L or Trc-S292E but enhanced by Trc-K122A/T453A. Mitochondrial morphology was monitored with a mito-GFP reporter. Bar, 30 μm. (*D*,*E*) $PINK1^{B9}$ mutation-induced mitochondrial aggregation in DNs (*D*) or loss of DNs in the PPL1 clusters (*E*) was strongly rescued by *TH-Gal4*-driven expression of wild-type or constitutively active Trc but enhanced by dominant-negative Trc. Bar, 5 μm. (*F*) Western blot analysis showing the effects of PINK1 LOF or overexpression on Trc phosphorylation. Trc-L overexpression served as a positive control. (*G*) In vitro kinase assay showing the effects of PINK1 LOF or overexpression on Trc kinase activity. Trc-L purified from control, PINK1 mutant, and PINK1-overexpressing animals was tested for kinase activity using AAK1-HA as a substrate in the presence of ATP-γ-S and phosphorylation detected by anti-thiophosphate ester antibody after esterification with p-nitrobenzylmesylate (PNBM). (P.C.) Positive control with extract added; (N.C.) negative control with no kinase added. Bar graph shows data quantification. (*H*) Western blot analysis showing that PINK1-induced Trc phosphorylation of T453 was Rictor-dependent, whereas that of S292 was Rictor-independent. (*) $P < 0.05$; (***) $P < 0.005$ in one-way ANOVA tests in *E* and *G*.

nylhydrazone (CCCP)-treated HeLa cells, NDR1 was found to colocalize with Parkin and the mitochondrial outer membrane marker Tom 20 (Supplemental Fig. S9B), suggesting that NDR1 might also be localized to mitochondria to exert MQC. In Parkin stably transfected HeLa cells that were subjected to Rictor RNAi (Supplemental Fig. S11A,D) or in $rictor^{-/-}$ MEF cells (Supplemental Fig. S11B,C,E), the recruitment of Parkin to damaged mitochondria and the kinetics of mitophagy were also delayed, supporting a critical role of mTORC2 in PINK1/Parkin-directed mitophagy in mammals.

We further investigated the mechanism of action of NDR1 in mammalian cells. It has been reported that Parkin is phosphorylated and activated by phosphorylation upon CCCP treatment (Kondapalli et al. 2012; Shiba-Fukushima et al. 2012). In HeLa cells stably transfected with Parkin, CCCP treatment led to increased phosphorylation of NDR1 and Parkin as detected with Phos tag. NDR1 RNAi significantly attenuated Parkin phosphorylation (Supplemental Fig. S12A), consistent with Parkin acting downstream from NDR1. Further supporting this notion, the activity of Parkin as measured by its autoubiquitination was reduced by NDR1 RNAi (Supplemental Fig. S12B). Moreover, the destabilization of MQC-related proteins Mfn1 and Miro1 by CCCP-activated PINK1/Parkin signaling was significantly attenuated by NDR1 RNAi (Supplemental Fig. S12A). These results support the notion that, as in flies, NDR1 kinase signaling acts upstream of Parkin and the other key MQC players in the mammalian MQC pathway.

Our results demonstrate that mTORC2 and Trc signaling are actively involved in the dynamic MQC network directed by PINK1 and that they act between PINK1 and Parkin in a conserved signaling pathway. This finding reveals a previously unappreciated complexity in the signaling steps between PINK1 and Parkin. This is the first time both mTORC2 and Trc are directly implicated in MQC. The fact that PINK1 regulates Trc T453 phosphorylation in an mTORC2-dependent manner and S292 phosphorylation in an mTORC2-independent manner suggests the involvement of additional kinases in this MQC pathway. Our finding of active p-Trc localizing primarily to mitochondria suggests that mitochondria may serve as a key platform for Trc signaling. The kinase that directly acts on Trc T453 in the context studied here remains to be identified. Although mTORC2 is required, it may not be the kinase that directly phosphorylates this site (Koike-Kumagai et al. 2009). Similarly, although PINK1 is required for mTORC2 activation, our results suggest that PINK1 acts through maintaining mitochondrial CI activity to influence mTORC2 activity, rather than directly phosphorylating mTORC2 as proposed in a previous study (Murata et al. 2011). Our findings offer new insights into the novel role of mitochondria in regulating mTORC2 and Trc/NDR kinase signaling.

mTORC2 and Trc signaling both induce cell morphology changes through actin cytoskeleton regulation (Jacinto et al. 2004; Fang and Adler 2010). Given the dynamic changes in mitochondrial distribution and morphology during MQC and the implicated roles of the actin cytoskeleton in regulating mitochondrial distribution and morphology (Boldogh and Pon 2006), it is possible that mTORC2/Trc may act in MQC through cytoskeletal regulation, although this remains to be tested. Our results support the notion that Trc signaling directly impinges on Parkin or the other key MQC executors (Supplemental Fig. S12C). A corollary of our finding is that mitochondrial localization of the kinases and the ensuing MQC may participate in other physiological processes regulated by mTORC2/Trc signaling. Given that deregulated mTORC2 (Zoncu et al. 2011), Trc/NDR (Cornils et al. 2011), and PINK1 and Parkin (Devine et al. 2011) signaling have all been linked to cancer in humans, another important implication of this study is that aberrant MQC signaling also contributes to cancerous growth and that therapeutic agents targeting the newly identified, highly conserved MQC signaling pathway may have broad therapeutic applications.

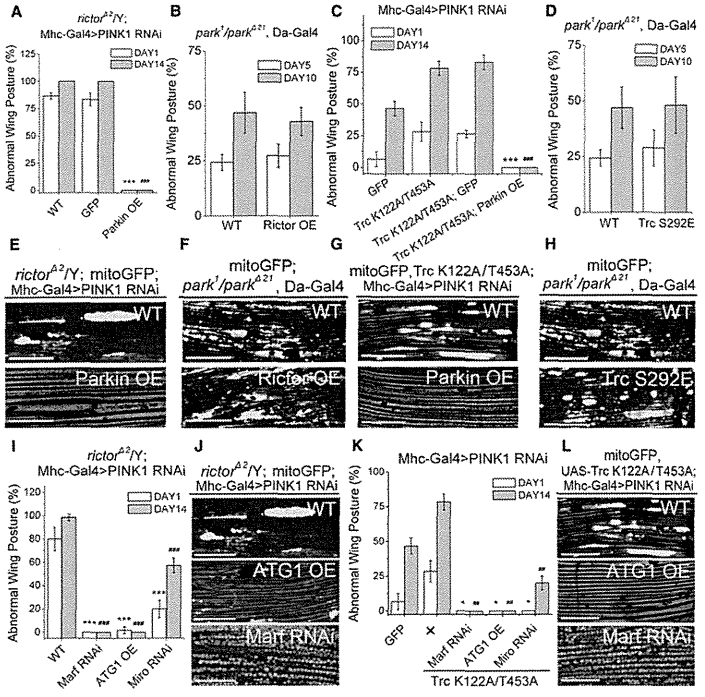

Figure 4. Genetic evidence that Parkin and MQC executors act downstream from TORC2 and Trc in the PINK1 pathway. (*A*,*E*) The enhancement of PINK1 RNAi-induced abnormal wing posture (*A*) or mitochondrial aggregation (*E*) by *rictor* deletion was suppressed by Parkin but not GFP overexpression. (*B*,*F*) The rescue of PINK1 RNAi-induced abnormal wing posture (*B*) or mitochondrial aggregation (*F*) by Rictor overexpression was blocked by Parkin LOF. (*C*,*G*) The enhancement of PINK1 RNAi-induced abnormal wing posture (*C*) or mitochondrial aggregation (*G*) by dominant-negative Trc was completely suppressed by Parkin but not GFP overexpression. (*D*,*H*) The rescue of PINK1 RNAi-induced abnormal wing posture (*D*) or mitochondrial aggregation (*H*) by wild-type or constitutively active Trc was blocked by Parkin LOF. (*I*,*J*) The enhancement of PINK1 RNAi-induced abnormal wing posture (*I*) or mitochondrial aggregation (*J*) by *rictor* deletion was suppressed by Miro-RNAi, Marf-RNAi, or Atg1 overexpression. (*K*,*L*) The enhancement of PINK1 RNAi-induced abnormal wing posture by dominant-negative Trc was suppressed by Miro-RNAi, Marf-RNAi, or Atg1 overexpression. (* or #) $P < 0.05$; (** or ##) $P < 0.01$; and (*** or ###) $P < 0.005$ in one-way ANOVA or Student's *t*-tests when data from day 1 (*) or day 14 (#) were compared. Bars: *E–F*,*J*,*L*, 30 μm.

Materials and methods

GST fusion protein preparation

The construct expressing human GST-AKT-KD used as the substrate in the in vitro TORC2 kinase assays was a gift from Dr. Dianqing Wu. To avoid autophosphorylation of AKT, the Lys179 and Thr308 residues were mutated (Gan et al. 2011). GST fusion protein was expressed in the *Escherichia coli BL21 (DE3)* strain and purified using glutathione-agarose beads following standard protocols.

Immunoprecipitation and kinase assay of TORC2

For TORC2 immunoprecipitation, methods adopted from previous studies (Koike-Kumagai et al. 2009; Gan et al. 2011) were used. Briefly, flies were crossed and raised in standard medium at 25°C. Male flies expressing Flag-tagged Sin1 were collected and homogenized in lysis buffer (40 mM HEPES at pH 7.5, 120 mM NaCl, 0.3% CHAPS, 1 mM EDTA, 10 mM β-glycerophosphate, 50 mM NaF, 1 mM PMSF). TORC2 was immunoprecipitated by incubating the supernatant with pre-equilibrated anti-Flag M2 beads (Sigma Aldrich) for 3 h at 4°C. Immunocomplexes were washed 3 times in lysis buffer and twice with the TORC2 kinase buffer (25 mM HEPES at pH 7.5, 100 mM KAc, 2 mM $MgCl_2$). The integrity of the TORC2 was confirmed by Western blot analysis.

For kinase assays, TORC2 immunocomplexes were incubated with 500 ng of human GST-AKT-KD fusion protein in 30 μL of TORC2 kinase buffer containing 500 μM ATP. The reaction was performed for 30 min at 30°C and terminated by the addition of 30μL of 2× SDS sample buffer. AKT phosphorylation by TORC2 was analyzed by Western blot using the p-T473-AKT antibody (Cell Signaling Technology).

Mitochondrial and cytoplasmic protein fractionation

For mitochondria purification, we adopted a previous method (Kristian et al. 2006). Briefly, fly tissues were collected and homogenized in homogenization buffer (210 mM mannitol, 70 mM sucrose, 1 mM EGTA, 10 mM β-glycerophosphate, 50 mM NaF, 1 mM PMSF, 5 mM HEPES at pH 7.12). The homogenate was centrifuged at 1500*g* for 5 min, and the supernatant was collected and centrifuged again at 13,000*g* for 17 min. The supernatant was concentrated as a cytoplasmic protein sample, and the pellet was stored for further mitochondrial purification. For mitochondrial purification, the previous pellet was resuspended in 15% Percoll solution and loaded onto a 15%–22%–50% discontinuous Percoll gradient. The gradient was centrifuged at 30,700*g* for 6 min, and intact mitochondria were recovered from the 22%–50% gradient interface. Mitochondria were washed with homogenization buffer and subjected to SDS-PAGE.

Quantitative Western blot analysis

To obtain quantitative Western blot results, experimental conditions such as the amounts of protein loaded, the antibody dilutions, and exposure times were adjusted to make sure that the Western blot signals were in the linear range. For the in vitro kinase assays, Western blot analyses were performed using standard protocols. After incubation with the ECL reagent (PerkinElmer, Inc.), the signals were scanned using a Typhoon 9400 system (GE Healthcare Life Sciences), and signal intensity was quantified by ImageQuantTL. For the other immunoblots, the signals were recorded on X-ray film and scanned, and the signal intensity was analyzed by ImageQuantTL or ImageJ. Statistical analyses were based on data from three independent repeats.

Statistical analysis

Two-tailed Student's *t*-tests were used in the statistical analysis when comparing two samples. A one-way ANOVA test was used when multiple samples were compared.

Acknowledgments

We thank Dr. P. Aspenström, Dr. E. Baehrecke, Dr. R. Baloh, Dr. S. Birman, Dr. J. Chung, Dr. S. Cohen, Dr. K. Emoto, Dr. M. Guo, Dr. Y. Hata, Dr. S. Hatakeyama, Dr. B. Hemmings, Dr. Y.N. Jan, Dr. S. Konur, Dr. M. Magnuson, Dr. N. Matsuda, Dr. K. Nakagawa, Dr. W. Saxton, Dr. K. Tanaka, Dr. G. Thomas, Dr. P. Verstreken, Dr. D. Wu, Dr. K. Zinsmaier, Bloomington *Drosophila* Stock Center, Vienna *Drosophila* RNAi Center, and TRiP at Harvard Medical School (NIH/NIGMS R01-GM084947) for flies and reagents, and Lu laboratory members for technical help and discussions. This work was supported by the NIH (R01AR054926 and R01MH080378 to B.L.), Grant-in-Aid for Young Scientists (B) from MEXT in Japan (to Y.I.), the CREST program of JST (to R.T.), a Grant-in-Aid for Scientific Research on Innovative Areas (to R.T.), and a Grant-in-Aid for Science Research from the Ministry of Health, Labor, and Welfare in Japan (to R.T.).

References

Boldogh IR, Pon LA. 2006. Interactions of mitochondria with the actin cytoskeleton. *Biochim Biophys Acta* **1763:** 450–462.